DRAFT VERSION: 22:36 ON SUNDAY 3RD MARCH, 2024
Preprint typeset using LaTeX style emulateapj v. 04/20/08

arXiv:1512.04551v3 [astro-ph.GA] 24 May 2016

FAINT COSMOS AGNS AT $Z \sim 3.3$ - I. BLACK HOLE PROPERTIES AND CONSTRAINTS ON EARLY BLACK HOLE GROWTH

B. TRAKHTENBROT[1,16], F. CIVANO[2,3], C. MEGAN URRY[2,4,5], K. SCHAWINSKI[1], S. MARCHESI[2,3,6], M. ELVIS[3], D. J. ROSARIO[7,8], H. SUH[9,3], J. E. MEJIA-RESTREPO[10], B. D. SIMMONS[11,12], A. L. FAISST[13,14], M. ONODERA[1,15]

Draft Version: 22:36 on Sunday 3rd March, 2024

ABSTRACT

We present new Keck/MOSFIRE *K*-band spectroscopy for a sample of 14 faint, X-ray-selected active galactic nuclei (AGNs) in the COSMOS field. The data cover the spectral region surrounding the broad Balmer emission lines, which enables the estimation of black hole masses ($M_{\rm BH}$) and accretion rates (in terms of $L/L_{\rm Edd}$). We focus on 10 AGNs at $z \simeq 3.3$, where we observe the Hβ spectral region, while for the other four $z \simeq 2.4$ sources we use the Hα broad emission line. Compared with previous detailed studies of unobscured AGNs at these high redshifts, our sources are fainter by an order of magnitude, corresponding to number densities of order $\sim 10^{-6} - 10^{-5}\,{\rm Mpc}^{-3}$. The lower AGN luminosities also allow for a robust identification of the host galaxy emission, necessary to obtain reliable intrinsic AGNs luminosities, BH masses and accretion rates. We find the AGNs in our sample to be powered by supermassive black holes (SMBHs) with a typical mass of $M_{\rm BH} \simeq 5 \times 10^8 M_{\odot}$ – significantly lower than the higher-luminosity, rarer quasars reported in earlier studies. The accretion rates are in the range $L/L_{\rm Edd} \sim 0.1 - 0.4$, with an evident lack of sources with lower $L/L_{\rm Edd}$ (and higher $M_{\rm BH}$), as found in several studies of faint AGNs at intermediate redshifts. Based on the early growth expected for the SMBHs in our sample, we argue that a significant population of faint $z \sim 5 - 6$ AGNs, with $M_{\rm BH} \sim 10^6 M_{\odot}$, should be detectable in the deepest X-ray surveys available, but this is *not* observed. We discuss several possible explanations for the apparent absence of such a population, concluding that the most probable scenario involves an evolution in source obscuration and/or radiative efficiencies.

Subject headings: galaxies: active — galaxies: nuclei — quasars: general

1. INTRODUCTION

While the local Universe provides ample evidence for the existence of supermassive black holes (SMBHs) with masses of $M_{\rm BH} \sim 10^6 - 10^{10} M_{\odot}$ in the centers of most galaxies (e.g., Kormendy & Ho 2013, and references therein), the understanding of their growth history relies on the analysis of accreting SMBHs, observed as active galactic nuclei (AGNs). Several studies and lines of evidence, mainly based on the observed redshift-resolved luminosity functions of AGNs, suggest that the epoch of peak SMBH growth occurred at $z \sim 2 - 3$, in particular in the sense of a peak in the integrated accretion density (e.g., Marconi et al. 2004; Hasinger et al. 2005; Ueda et al. 2014; Aird et al. 2015; Brandt & Alexander 2015, and references therein). Recent results from increasingly deep surveys have shown that at yet higher redshifts the number density and integrated emissivity of AGNs experience a marked decrease (e.g., Brusa et al. 2009; Civano et al. 2011; McGreer et al. 2013; Vito et al. 2014; Miyaji et al. 2015). Phenomenological "synthesis models" have been used to account for the observed evolution of the AGN population out to $z \sim 4 - 5$, particularly based on deep X-ray surveys (see, e.g., Gilli et al. 2007; Treister et al. 2009a; Ueda et al. 2014; Aird et al. 2015; Georgakakis et al. 2015). Broadly speaking, these synthesis models successfully reproduce the population of relic SMBHs in the local Universe, the X-ray background radiation, and the X-ray number counts. However, all these models depend on several simplifying assumptions, including the accretion rates, radiative efficiencies, and the shape of the X-ray spectral energy distribution (SED) of AGNs, among others. Our current understanding of the early growth of SMBHs is therefore still extremely limited. Most importantly, it lacks robust characterization of the distributions of the most basic physical properties of accreting SMBHs: black hole masses ($M_{\rm BH}$), accretion rates (in terms of $L/L_{\rm Edd}$ or $\dot{M}_{\rm BH}$) and radiative efficiencies (η; and/or BH spins, a_*), for SMBHs across a wide range of activity phases.

Reliable estimates of $M_{\rm BH}$, and therefore $L/L_{\rm Edd}$, from single-epoch spectra of AGNs at considerable redshifts rely

Electronic address: benny.trakhtenbrot@phys.ethz.ch
[1] Institute for Astronomy, Department of Physics, ETH Zurich, Wolfgang-Pauli-Strasse 27, CH-8093 Zurich, Switzerland
[2] Yale Center for Astronomy and Astrophysics, 260 Whitney Ave., New Haven, CT 06520-8121, USA
[3] Harvard-Smithsonian Center for Astrophysics, 60 Garden St., Cambridge, MA 02138, USA
[4] Department of Physics, Yale University, P.O. Box 208120, New Haven, CT 06520-8120, USA
[5] Department of Astronomy, Yale University, P.O. Box 208101, New Haven, CT 06520-8101, USA
[6] INAF–Osservatorio Astronomico di Bologna, via Ranzani 1, I-40127 Bologna, Italy
[7] Max-Planck-Institut für Extraterrestrische Physik (MPE), Postfach 1312, D-85741 Garching, Germany
[8] Department of Physics, Durham University, South Road, Durham DH1 3LE , UK
[9] Institute for Astronomy, University of Hawaii, 2680 Woodlawn Drive, Honolulu, HI 96822, USA
[10] Departamento de Astronomía, Universidad de Chile, Camino el Observatorio 1515, Santiago, Chile
[11] Oxford Astrophysics, Denys Wilkinson Building, Keble Road, Oxford OX1 3RH, UK
[11] Oxford Astrophysics, Denys Wilkinson Building, Keble Road, Oxford OX1 3RH, UK
[13] Infrared Processing and Analysis Center, California Institute of Technology, Pasadena, CA 91125, USA
[14] Cahill Center for Astronomy and Astrophysics, California Institute of Technology, Pasadena, CA 91125, USA
[15] Subaru Telescope, National Astronomical Observatory of Japan, 650 North A'ohoku Place, Hilo, HI 96720, USA
[16] Zwicky Postdoctoral Fellow

on the careful analysis of either the spectral regions surrounding either the Hβ, Hα, or Mg II λ2798 broad emission lines, and on the results of reverberation mapping campaigns. Other emission lines, which may potentially enable the estimation of $M_{\rm BH}$ in tens of thousands of quasars from the Sloan Digital Sky Survey (SDSS), up to $z\sim5$ (e.g., C IV λ1549), are known to be problematic (e.g., Baskin & Laor 2005; Shen et al. 2008; Fine et al. 2010; Shen & Liu 2012; Trakhtenbrot & Netzer 2012; Tilton & Shull 2013). Therefore, at $z\gtrsim2$, the study of the evolution of $M_{\rm BH}$ practically requires near-IR (NIR) spectroscopy, and ground-based studies are thus limited to specific redshift bands, at $z\sim2.1-2.7$, $3.1-3.8$, $4.6-4.9$, and $6-7.2$. Several studies followed this approach with relatively small samples of optically selected, high-luminosity unobscured AGNs, mostly focusing on the most luminous sources at each redshift bin (e.g., Shemmer et al. 2004; Kurk et al. 2007; Netzer et al. 2007; Dietrich et al. 2009; Marziani et al. 2009; Willott et al. 2010; De Rosa et al. 2011; Trakhtenbrot et al. 2011). The studies of Shemmer et al. (2004) and Netzer et al. (2007) clearly show that the most massive BHs in the Universe, with $M_{\rm BH}\gtrsim10^{10}\,M_{\odot}$ (McConnell et al. 2011) are already in place by $z\sim3.5$, powering some of the most luminous quasars at $z\sim3-4$. Given their extreme masses, but modest accretion rates of $L/L_{\rm Edd}\simeq0.2$, these objects must have grown at higher rates at yet earlier epochs. Indeed, a population of SMBHs with $M_{\rm BH}\sim10^{9}\,M_{\odot}$ is now well established at $5\lesssim z\lesssim7$, presenting rapid, Eddington-limited accretion (e.g., Kurk et al. 2007; Willott et al. 2010; De Rosa et al. 2011; Trakhtenbrot et al. 2011; De Rosa et al. 2014). Thus, the extremely luminous $z\sim3-4$ quasars studied to date mark the final stage of the early, rapid growth of the most massive BHs in the Universe.

These results motivated the development of new models for the formation of high-mass BH seeds, at $z\gtrsim10$. Such processes, involving either dense stellar environments or direct collapse of gaseous halos, may lead to BH seeds with masses of up to $M_{\rm seed}\sim10^{4}$ or $10^{6}\,M_{\odot}$, respectively (see reviews by Volonteri 2010; Natarajan 2011, and references therein). Some models predict that such massive BH seeds are sufficiently abundant in the early Universe to easily account for the rare $M_{\rm BH}\sim10^{9}\,M_{\odot}$ quasars observed at $z>3$ (see, e.g., Dijkstra et al. 2008; Agarwal et al. 2013). Several other recent studies have instead focused on extremely efficient accretion onto seed BHs, as an alternative (or complementary) explanation for the highest-redshift quasars (e.g., Alexander & Natarajan 2014; Madau et al. 2014). It is possible that these rare, extremely luminous and massive quasars have indeed grown from high-mass BH seeds and/or by extreme accretion scenarios, while the majority of high-redshift SMBHs, detected as lower-luminosity AGNs, can be explained by stellar remnants, with $M_{\rm seed}\lesssim100\,M_{\odot}$. The only way to observationally test these scenarios and seeding models would be to constrain the distributions of $M_{\rm BH}$ (and $L/L_{\rm Edd}$) in large samples of AGNs, which extend toward low luminosities and thus significant number densities. Moreover, these distributions should be established at the highest possible redshifts, since at later epochs the initial conditions of BH seed formation are completely "washed out," partially due to the increasing importance of "late seeding" (e.g., Schawinski et al. 2011; Bonoli et al. 2014). Such distributions would in turn enable the direct study of the progenitors of the typical luminous SDSS $z\sim1-2$ quasars, which have already accumulated most of their final mass.

Since wide optical surveys (e.g., SDSS) only probe the rarest, most luminous (and least obscured) sources at $z>2$, they cannot provide the parent samples required for mapping the distributions of $M_{\rm BH}$ and $L/L_{\rm Edd}$. The most up-to-date determinations of the AGN luminosity function at these high redshifts indicate that the most luminous quasars have number densities of order $\Phi\sim10^{-8}\,{\rm Mpc}^{-3}$, while AGNs that are fainter by an order of magnitude are more abundant by at least a factor of 20 (e.g. Glikman et al. 2010; Ikeda et al. 2011; Masters et al. 2012; McGreer et al. 2013). The best sources for samples of these fainter AGNs are deep, multi-wavelength surveys, with appropriate X-ray coverage, such as the COSMOS and CDF-S surveys (Civano et al. 2016 and Xue et al. 2011, respectively; see Brandt & Alexander 2015 for a recent review). In such surveys, moderate-luminosity AGNs ($L_{\rm X}\gtrsim few\times10^{43}\,{\rm erg\,s^{-1}}$) can be detected at redshifts as high as $z\sim5$, as confirmed by spectroscopic follow-up campaigns (e.g., Szokoly et al. 2004; Trump et al. 2009b; Silverman et al. 2010; Civano et al. 2011; Vito et al. 2013; Marchesi et al. 2015, M15 hereafter). Furthermore, the multi-wavelength data available in these deep fields can provide a large suite of ancillary information relevant to the evolution of the central accreting SMBHs, ranging from the accretion process and the central engine (i.e., X-ray spectral analysis) to the properties of the host galaxies (e.g., the masses and sizes of the stellar components and/or the presence of cold gas).

We therefore initiated a dedicated project to measure BH masses, accretion rates, and host galaxy properties in a sample of moderate-luminosity, $z\sim2.1-3.7$ AGNs, located within the COSMOS field (Scoville et al. 2007), and selected through the extensive X-ray coverage provided by the relevant *Chandra* surveys (Elvis et al. 2009; Civano et al. 2016). In this paper we present new Keck/MOSFIRE NIR spectroscopy and determinations of $M_{\rm BH}$ and $L/L_{\rm Edd}$ for a sample of 14 such objects. In Section 2 we describe the observations, data reduction, and analysis, including the estimates of $M_{\rm BH}$ and $L/L_{\rm Edd}$. In Section 3 we compare these, and other probes of SMBH evolution, to those found for more luminous quasars, and examine the relevance of high-mass BH seeding models to lower-luminosity AGNs. We summarize the main findings of this study in Section 4. We note that one particularly intriguing object in our sample (CID-947) was discussed extensively in a previous, separate publication (Trakhtenbrot et al. 2015, T15 hereafter). Throughout this work we assume a cosmological model with $\Omega_{\Lambda}=0.7$, $\Omega_{\rm M}=0.3$, and $H_0=70\,{\rm km\,s^{-1}\,Mpc^{-1}}$.

2. SAMPLE, OBSERVATIONS, AND DATA ANALYSIS

2.1. *Sample Selection and Properties*

This study focuses on 14 AGNs, selected from the X-ray *Chandra* catalog of the COSMOS field. The *Chandra* data combine the *Chandra*-COSMOS survey (Elvis et al. 2009; Civano et al. 2012), and the more recent *Chandra COSMOS Legacy* survey (Civano et al. 2016; Marchesi et al. 2016). We note that all 14 sources are also detected in the *XMM-Newton* X-ray survey of the COSMOS field (Hasinger et al. 2007, see below). We selected sources that are robustly classified as broad-line AGNs at $z\simeq3-3.7$, based on the (optical) spectroscopic surveys of the COSMOS field (Lilly et al. 2007, 2009; Trump et al. 2009b). The chosen redshift range ensures that the spectral region surrounding the Hβ broad emission line will be observed in the *K*-band. Adequate coverage of this spectral region is essential for the estimation of

$M_{\rm BH}$ (e.g., Trakhtenbrot & Netzer 2012; Shen 2013). All the sources are robustly detected in the K-band, based on the UltraVISTA DR2 catalog (see survey description in McCracken et al. 2012). To ensure an adequate signal-to-noise ratio (S/N) within a reasonable observation time, we further focused on those $z \simeq 3-3.7$ COSMOS AGNs that meet a flux limit of $K_{\rm AB} \leq 21.5$, resulting in 14 targets in the range $20 < K_{\rm AB} < 21.5$. Four additional broad-line AGNs at $z \simeq 2.4$ were selected to be observed in parallel to (some) of the primary targets, within the same MOSFIRE masks. For these four sources, the K-band covers the Hα broad emission line, which can also be used for $M_{\rm BH}$ estimates (through secondary calibration; see, e.g., Greene & Ho 2005). These slightly brighter sources ($19.2 < K_{\rm AB} < 20.1$) were drawn from a much larger population of X-ray-selected, unobscured COSMOS AGNs at this redshift band, solely based on their (angular) proximity to the primary $z \simeq 3.3$ AGNs. As such, they do *not* represent the general population of $z \simeq 2.4$ AGNs. The UltraVISTA K-band fluxes are further used here to test the absolute flux calibration of the MOSFIRE spectra (see Section 2.2 below).

The (full band) X-ray fluxes of the sources span about a factor of 15, $f_{[0.5-10\,{\rm keV}]} \sim (2.2-32)\times10^{-15}\,{\rm erg\,cm^{-2}\,s^{-1}}$, corresponding to rest-frame hard-band luminosities of $L_{[2-10\,{\rm keV}]} \sim (7.3-97)\times10^{43}\,{\rm erg\,s^{-1}}$, as reported in M15. These X-ray fluxes are high enough to allow for a robust detection of *all* of our sources in the *XMM*-COSMOS survey (Hasinger et al. 2007; Brusa et al. 2010). We compare the *Chandra*- and *XMM*-based X-ray luminosity measurements in Section 2.3 below. Basic information regarding the sources and the observations (detailed below) is provided in Table 1. The $z = 3.328$ AGN CID-947 was analyzed and published separately in T15, because it exhibits several intriguing features, including an extremely high BH mass, extremely low accretion rate, and an AGN-driven outflow, among others. In many parts of the present study we will mention CID-947 separately, as its properties differ from the rest of our sample.

The K-band magnitudes of our sources can be used to estimate a lower limit to the BH masses and accretion rates we might expect to find, using the methods detailed in Section 2.5. At $z = 3.3$, the chosen flux limit ($K_{\rm AB} \simeq 21.5$) translates to $L_{5100} \simeq 1.1\times10^{45}\,{\rm erg\,s^{-1}}$ and $L_{\rm bol} \simeq 7\times10^{45}\,{\rm erg\,s^{-1}}$, assuming the composite quasar spectrum of Vanden Berk et al. (2001), and the L_{5100}-dependent bolometric correction introduced in Trakhtenbrot & Netzer (2012, see Section 2.5). Further assuming that the width of the Hβ line is in the range $1500 < {\rm FWHM\,(H}\beta) < 15000\,{\rm km\,s^{-1}}$, we obtain lower limits of $M_{\rm BH} \gtrsim 5.5\times10^{7}\,M_{\odot}$ and of $L/L_{\rm Edd} \gtrsim 0.008$. [17]

Compared to previous studies of $M_{\rm BH}$ and $L/L_{\rm Edd}$ in $z\sim3-4$ AGNs (Shemmer et al. 2004; Netzer et al. 2007), our sample covers lower luminosities. The rest-frame UV luminosities of our $z \simeq 3.3$ sources, measured from the optical spectra, are in the range $L_{1450} = (0.8-13)\times10^{45}\,{\rm erg\,s^{-1}}$ ($M_{1450} = -25.4$ to -22.4; see Table 2). The typical UV luminosities are fainter, by about a factor of 6, than those probed in previous studies. Our sample therefore represents a much more abundant AGN population. In Figure 1 we present the luminosity function of unobscured, $z \sim 3.2$ AGNs determined by Masters et al. (2012), which relies on COSMOS AGNs similar to the parent sample of our sources. The luminosity regimes probed by our sample, and the previously studied samples, are marked. The integrated number density of sources within the luminosity range we target is $\Phi \simeq 2.5\times10^{-6}\,{\rm Mpc^{-3}}$, higher by a factor of about 25 than that of the more luminous, previously studied objects (for which $\Phi \simeq 10^{-7}\,{\rm Mpc^{-3}}$).

As our sample is defined through a combination of several criteria, it is worth bearing in mind the possible selection biases. First, the *Chandra*-based X-ray selection should include all Compton-thin AGNs above the survey flux limit (i.e., $N_{\rm H} \lesssim 10^{23}\,{\rm cm^{-2}}$; see M15). Several studies have highlighted the presence of obscured AGN emission in high-redshift sources (e.g., Fiore et al. 2008; Treister et al. 2009b). Next, the X-ray AGNs must be associated with an optical and NIR counterpart, and have optical spectroscopy for redshift determination and classification as broad-line AGNs. In principle, this would mean that dust-rich (but Compton-thin) systems, such as "red quasars" (e.g., Banerji et al. 2015; Glikman et al. 2015), may be missed by our sample selection criteria. However, the M15 compilation of high-z AGNs in the *Chandra COSMOS Legacy* survey notes that only about 40 X-ray sources among the 4016 X-ray-selected sources ($\sim1\%$) in the entire survey lacked i-band counterparts, with about half of those lacking also K-band counterparts. For most COSMOS AGNs the spectral information is based on the zCOSMOS-bright survey (see Table 1), which imposes an optical flux limit of $i_{\rm AB} < 22.5$ (Lilly et al. 2007). Additional spectroscopic follow-up available for COSMOS (X-ray) AGNs provides several other $z > 3$ X-ray-selected broad-line sources with $i_{\rm AB} < 25$, well beyond the zCOSMOS limit. These are, however, generally too faint to be included in our sample in terms of the K-band cut we imposed, motivated by the need to observe a sizable sample. We conclude that our sample is highly representative of the population of unobscured COSMOS AGNs at $z \simeq 3-3.7$, down to a flux limit of $K_{\rm AB} \simeq 21.5$. As the sample is mainly limited by (rest-frame) UV and optical flux selection, it may only be biased against highly obscured AGNs, either in the X-rays or in the (rest-frame) UV. Such "missed" AGNs may be indeed powered by SMBHs with $M_{\rm BH}$ and/or $L/L_{\rm Edd}$ that are higher than the aforementioned lower limits.

2.2. *Observations and Data Reduction*

The Keck/MOSFIRE (McLean et al. 2012) observations were allocated through the Yale-Caltech collaborative agreement, and conducted during six nights in the period between 2014 January and 2015 February. Observational conditions during 5 of the nights were generally good, with typical seeing of $\sim1''$ (or $\sim0.''8$ in the NIR), but also with some periods of high humidity and cloud cover. One night was completely lost due to poor weather. Our campaign targeted all the 14 primary $z \simeq 3.3$ targets we selected, except for one source (LID-283). The targets were observed as part of 12 different MOSFIRE masks, with the four secondary $z \simeq 2.4$ sources being observed within (some of) the masks designed to include the primary $z \simeq 3.3$ ones. To ensure adequate coverage of the sky background emission, and its subtraction from the AGN signal, the sources studied here were observed through two or three MOSFIRE (pseudo-)slits, corresponding to $14''$ or $21''$, respectively. We set the slits to have widths of $0.''7$-$1''$, depending on the seeing. This translates to a spectral resolution of $\sim 2500-3600$ ($80-120\,{\rm km\,s^{-1}}$), which is adequate for studies of broad and narrow emission lines in un-

[17] Note that these limits are strongly (anti-)correlated, i.e., sources with $M_{\rm BH} \sim 6\times10^{7}\,M_{\odot}$ and $L/L_{\rm Edd} \sim 0.01$ would be significantly fainter than our chosen flux limit. See Figure 5.

TABLE 1
OBSERVATION LOG

Subsample	Object ID X-ray[a]	Object ID Galaxy ID[b]	R.A. (deg)	Decl. (deg)	z[c]	Optical Spec.[c]	K_{AB} mag.[d] (ref.)	K_{AB} mag.[d] (syn.)	MOSFIRE Exp. Time (s)	S/N[e]	Comments
$z \simeq 3.3$	CID-349	1294973	150.004380	2.038898	3.5150	zCOSb	21.238	21.277	9000	7	...
	CID-413	2039436	149.869660	2.294046	3.3450	zCOSb	20.134	20.472	5400	9	...
	CID-113	2350265	150.208850	2.481935	3.3330	zCOSb	19.555	19.774	6840	16	...
	CID-947	1593500	150.297250	2.148846	3.3280	zCOSb	20.052	20.045	3600	8	...
	LID-775	3176366	149.472888	2.793379	3.6260	IMACS	21.488	21.442	14400	6	...
	LID-1638	1462117	150.735585	2.199557	3.5030	VVDS	19.651	19.736	3600	15	...
	LID-205	2665989	150.240801	2.659037	3.3560	zCOSb	21.197	21.245	10800	8	...
	LID-499	2534376	150.737172	2.722557	3.3020	zCOSb	20.215	20.378	2520	6	...
	LID-460	2583306	150.620069	2.671382	3.1430	zCOSb	19.865	20.356	4860	22	...
	LID-721	2137194	149.529103	2.380143	3.1080	IMACS	20.157	20.010	3600	9	...
$z \simeq 2.4$	LID-496	2577949	150.720703	2.693635	2.6298	SDSS	20.116	20.225	2520	6	with LID-499
	LID-504	2530857	150.767390	2.739021	2.2220	zCOS	19.670	19.736	2520	8	with LID-499
	LID-451	2592676	150.705563	2.629612	2.1225	SDSS	19.178	19.238	4860	17	with LID-460
	CID-352	1300441	150.058920	2.015179	2.4980	SDSS	19.201	19.369	9000	22	with CID-349

[a] X-ray object IDs correspond to either the C-COSMOS ("CID") or *Chandra COSMOS Legacy* survey catalogs ("LID") (Elvis et al. 2009 and Civano et al. 2016, respectively).
[b] COSMOS galaxy IDs correspond to those given by Capak et al. (2007).
[c] Redshifts are obtained from rest-frame UV emission lines, observed through optical spectroscopy, from either the zCOSMOS-bright ("zCOSb"; Lilly et al. 2007), IMACS (Trump et al. 2009b), VVDS (Fevre et al. 2013), or SDSS (DR7; Abazajian et al. 2009) observations of the COSMOS field.
[d] K-band magnitudes obtained from the UltraVISTA survey ("ref." column, McCracken et al. 2012) and from synthetic photometry of the calibrated MOSFIRE spectra.
[e] Median signal-to-noise ratios, calculated per spectral bin of 1 Å in the rest frame ($\sim 45-60\,\mathrm{km\,s^{-1}}$).

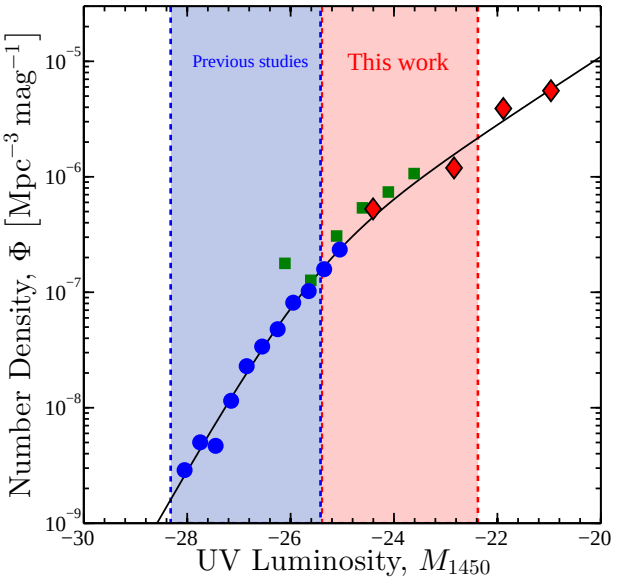


FIG. 1.— The luminosity function of unobscured AGNs at $z \sim 3-3.5$, reproduced from the study of Masters et al. (2012), including the best-fit double power-law model (black line). The red diamonds represent COSMOS AGNs, similar to the parent sample from which our targets are drawn. Blue circles at higher luminosities are taken from the SDSS (Richards et al. 2006), while the green squares in the overlap region are taken from the SWIRE survey (Siana et al. 2008). Other samples and error bars from all data points are omitted for clarity. The shaded regions represent the luminosity regimes covered by our sample (red) and previous studies of $M_{\rm BH}$ and $L/L_{\rm Edd}$ in luminous $z \sim 3-4$ AGNs (blue; Shemmer et al. 2004; Netzer et al. 2007). Our sample probes a much more representative population of $z \simeq 3.3$ AGNs, with an integrated number density that is higher by a factor of about 25 than the previously studied objects.

obscured AGNs. The rest of the slits in the MOSFIRE masks were allocated to a wide variety of other COSMOS targets, totaling 225 targets and including many X-ray-selected AGNs that lack redshift determinations. Those data will be analyzed and published separately. We also observed several A0V stars (HIP34111, HIP43018, HIP56736, and HIP64248) as well as the fainter white dwarf GD71, at least twice during each night to allow robust flux calibration.

We reduced the data using a combination of different tools. First, we used the dedicated MOSFIRE pipeline[18] to obtain flat-fielded, wavelength-calibrated 2D spectra of all the sources observed within each mask (including the standard stars). The wavelength calibration was performed using sky emission lines, and the best-fit solutions achieved a typical rms of ∼0.1 Å. Next, we used standard `IRAF` procedures to produce 1D spectra, using apertures in the range of 4-6 pix (i.e., $0\farcs72-1\farcs1$). Finally, we used the `Spextool` IDL package to remove the telluric absorption features near 2 μm and to perform the relative and absolute flux calibrations, based on a detailed spectrum of Vega (Vacca et al. 2003; Cushing et al. 2004). We verified that the resulting spectra do not have any significant residual spectral features, which might have been misinterpreted as real, AGN-related emission or absorption features.

To test the reliability of our flux calibration procedure, we have calculated the synthetic magnitudes of the calibrated spectra (using the UltraVISTA K-band filter curve). The synthetic magnitudes are generally in good agreement with the reference UltraVISTA magnitudes, with differences of less than 0.2 mag for 11 of the 14 sources in the final sample. The remaining three sources have flux differences of less than 0.5 mag. Such differences can be explained by intrinsic AGN variability, which for the roughly year-long timescales probed here is expected to be ∼0.2-0.5 mag (e.g., Vanden Berk et al. 2004; Wilhite et al. 2008; Morganson et al. 2014). We do, however, note that our calibrated spectra are *systematically* fainter than the reference imaging-based fluxes, by about 0.1 mag. In any case, since $M_{\rm BH} \sim L^{0.65}$ and $L/L_{\rm Edd} \sim L^{0.35}$ (see Section 2.5), these flux differences correspond to uncertainties of less than ∼0.1 dex, and most probably ∼0.05 dex, on the estimated basic physical properties of the SMBHs un-

[18] Version 1.1, released 2015 January 6. See: http://github.com/Keck-DataReductionPipelines/MosfireDRP

der study. This is much smaller than the systematic uncertainty associated with the "virial" $M_{\rm BH}$ estimator used here (see Shen 2013, and Section 2.5)

For the source CID-349 we have combined two calibrated 1D spectra, originating from two consequent observing blocks, the second of which was considerably shorter and of poorer quality than the first one, due to varying observing conditions. This was done by binning the spectra in bins of 2 pixels (i.e., $\sim$1 Å in the rest frame), combining the spectra through a weighted average (based on their noise spectra), and then median-smoothing the combined spectrum over 5 pixels ($\sim$ 5 Å in the rest frame), to avoid single-pixel features inherited from the shorter and poorer-quality observing block. Based on our experience with modeling such data, we are confident that the particular choices made in these binning and smoothing steps have little effect on the deduced spectral models and parameters, because these are mainly driven by the width of the broad Balmer lines, which is of the order of a few thousand km s^{-1} ($\sim$50 Å in the rest frame). Two of the fainter sources we observed (CID-955 and CID-1311) resulted in spectra that were too noisy to be used for the detailed spectral analysis required for the estimation of $M_{\rm BH}$. The reduced spectrum of another (optically faint) source, LID-1710, included no identifiable emission lines. Otherwise, the calibrated spectra of the remaining 14 sources, at both redshift bands, typically have S/N $\sim 5-7$ per instrumental spectral pixel (of about 2.2 Å). After rebinning the spectra to a uniform resolution of 1 Å in the rest frame (corresponding to $\sim 45-60\,{\rm km\,s^{-1}}$), this results in S/N $\sim 7-10$, with some of the brighter sources reaching $S/N \sim 15-20$. These (median) values of S/N per spectral bin of 1 Å (in the rest frame) are listed in Table 1. The final forms of the spectra of the 14 sources studied here are presented in Figures 2 and 3.

2.3. *Ancillary Data*

To obtain an independent constraint on intrinsic AGN-dominated luminosities, we relied on the X-ray data available for all sources from the *Chandra* catalogs in the COSMOS field (M15, Marchesi et al. 2016). These rest-frame 2-10 keVluminosities, L_{2-10}, were obtained directly from the soft-band fluxes (0.5-2 keV), which at the redshift range of our sources probe the rest-frame hard-band (2-10 keV) photons. We assumed a power-law SED with a photon index of $\Gamma = 1.4$, for consistency with the analysis of the parent sample of high-redshift AGNs in the *Chandra COSMOS Legacy* survey (M15). As mentioned above, the X-ray luminosities we thus obtain are in the range of $\log\left(L_{2-10}/{\rm erg\,s^{-1}}\right) = 43.9-45$ (see Table 2). As previously noted, all the sources in our sample are robustly detected in the *XMM*-COSMOS survey. We compared the *Chandra*-based X-ray luminosities to those determined from the *XMM-Newton* data, as described in Brusa et al. (2009). The *Chandra* luminosities agree with the *XMM* ones, with a median offset of 0.07 dex (i.e., *Chandra*-based luminosities are typically higher). This difference is probably due to the different assumptions made in deriving the *XMM*-based luminosities, particularly the power law of the X-ray SED ($\Gamma = 1.7$ in Brusa et al. 2009 versus 1.4 here).

Finally, we used data from the COSMOS/VLA radio survey (Schinnerer et al. 2010) to determine whether the sources in our sample are radio-loud (RL) AGNs. The energy output of such RL-AGNs may be dominated by jets, and several studies have suggested that their BH masses may be systematically higher than those of the general population, perhaps due to the nature of their host galaxies (e.g., McLure & Jarvis 2004). Four sources in our sample are robustly detected at 1.4 GHz (i.e., above 5σ; CID-113, LID-1638, LID-499, and LID-451). We calculated the radio loudness parameter, $R_{\rm L} \equiv f_\nu\,(5\,{\rm GHz})\,/\,f_\nu\,({\rm optical})$, following Kellermann et al. (1989), and further assuming that the radio SED has the shape $f_\nu \propto \nu^{0.8}$. When comparing with the rest-frame optical fluxes (either from the spectral analysis detailed in Section 2.4, or the H-band UltraVISTA fluxes), we find that only the source LID-451 is a RL-AGN, with $R_{\rm L} \simeq 117$, and the source LID-460 is marginally RL, with $R_{\rm L} \simeq 10$.

2.4. *Spectral Analysis*

The spectra of the 14 sources with sufficiently high S/N were analyzed to obtain estimates of the continuum luminosity, and the luminosities and widths of the broad Balmer emission lines. The methodology of the analysis is very similar to that discussed in numerous previous works (e.g., Shang et al. 2007; Shen et al. 2011; Trakhtenbrot & Netzer 2012; **?**, and references therein) and is only briefly described here.

The spectra of the $z \simeq 3.3$ sources were modeled using the procedure presented in Trakhtenbrot & Netzer (2012). The model consists of a linear (pseudo) continuum, a broadened iron template, and a combination of Gaussians to account for the broad and narrow emission lines, namely He II, Hβ, [O III] λ4959 and [O III] λ5007. The continuum flux at 5100 Å was estimated directly from the best-fit linear continuum, which is performed in two narrow continuum bands, and used to measure the monochromatic continuum luminosity at (rest-frame) 5100 Å (L_{5100}). The broadened Fe II template (Boroson & Green 1992) is fitted in either the 4400-4650 or 5120-5200 Å spectral region,[19] and produces only negligible contamination to the 5100 Å continuum band. Most of the $z \simeq 3.3$ AGNs show very low levels of Fe II emission, although the limited quality of our spectra does not allow for a robust *measurement* of the physical properties related to this emission component. Finally, the Hβ line is modeled with two broad Gaussian components and a single narrow one, with the latter being tied to the [O III] features (in terms of linewidth). We note that the main different components are fitted in a serial manner: the best-fit continuum is subtracted from the original spectrum; the Fe II template is then fitted to the continuum-free spectrum, over a different wavelength range; the best-fit Fe II template is then subtracted, and finally the emission line model is fitted to the continuum- and iron-free spectrum. As for the $z \simeq 2.4$ sources, the Hα spectral complex was modeled using the procedure presented in **?**. The model consists of a linear (pseudo) continuum and a combination of Gaussians to account for Hα, [N II] $\lambda\lambda$6548, 6584 and [S II] $\lambda\lambda$6717, 6731. The Hα line is modeled with two broad Gaussian components and a single narrow one, again tied in width to the other nearby narrow emission lines. The luminosity of the broad Hα line is calculated from the best-fit model for the broad components of the line. All spectral fits were performed using the Levenberg–Marquardt algorithm for χ^2 minimization.

For the two Balmer lines, we preferred to use FWHM over $\sigma_{\rm BLR}$ as the probe of the virial velocity field of the broad-line region (BLR) gas, as the former can be more robustly estimated in spectra of moderate S/N, as is the case with

[19] For the two sources with $3 < z < 3.15$, LID-460 and LID-721, the MOSFIRE spectra do not cover the 4400-4650 Å spectral region (see Figure 2).

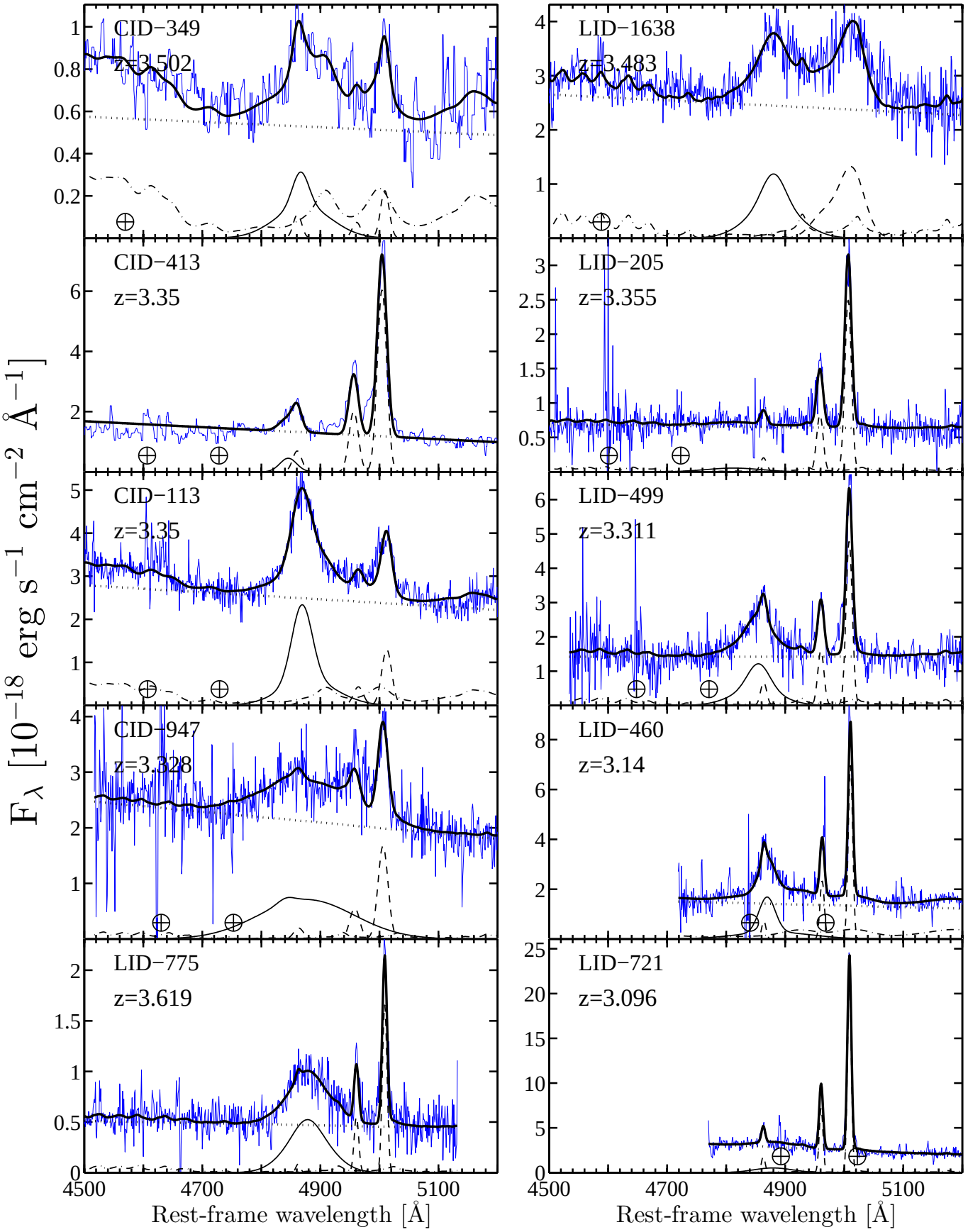


FIG. 2.— Keck/MOSFIRE spectra for the 10 X-ray-selected, $z \simeq 3.3$ COSMOS AGNs studied here (blue), along with the best-fitting spectral model (solid black lines). The data are modeled with a linear continuum (dotted), a broadened iron template (dotted-dashed), and a combination of narrow (dashed) and broad (thin solid) Gaussians. See Section 2.4 for details regarding the spectral analysis. Regions affected by telluric features are marked with encircled crosses. The spectra are shown prior to the host-light correction. Note the near absence of broad Hβ components in objects LID-205 and LID-721, and the peculiar broad [O III] profile in LID-1638 (see Section 3.1).

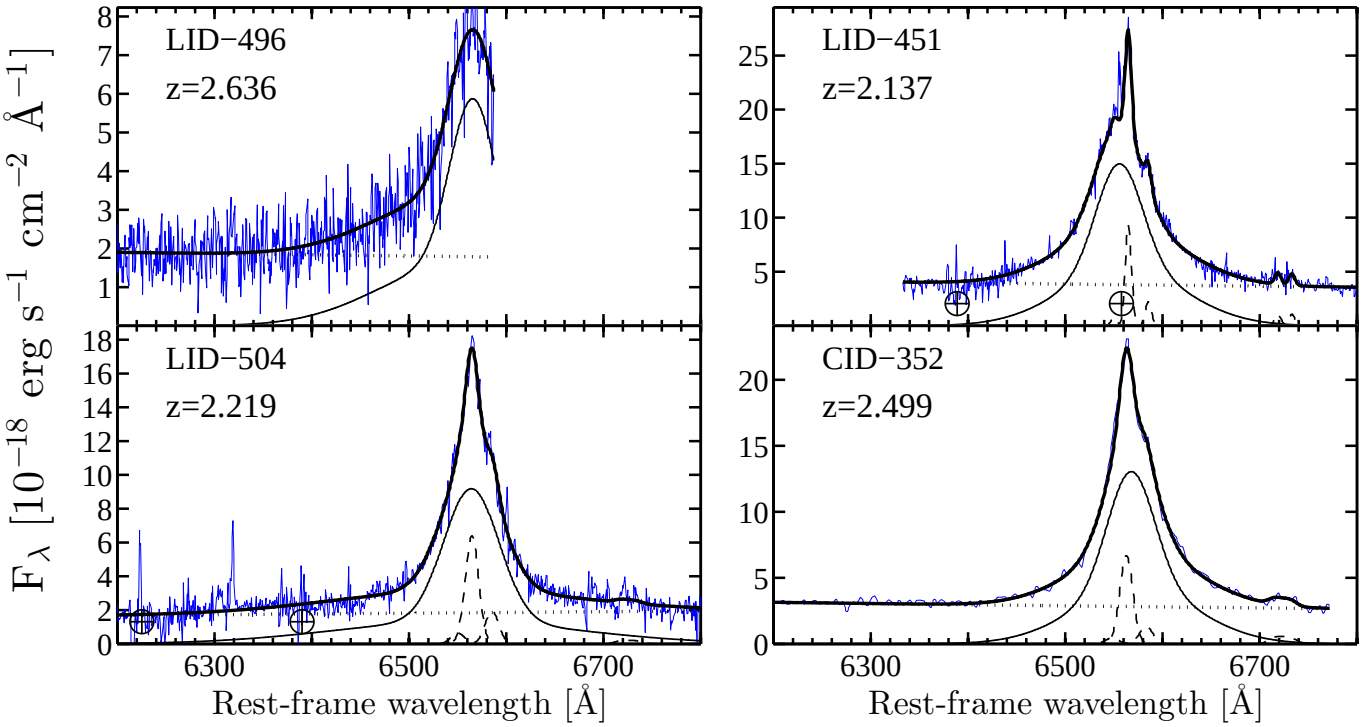


FIG. 3.— Keck/MOSFIRE spectra for the four X-ray-selected, $z \simeq 2.4$ COSMOS AGNs studied here (blue), along with the best-fitting spectral model (solid black lines). The data are modeled with a linear continuum (dotted), and a combination of narrow (dashed) and broad (thin solid) Gaussians. See Section 2.4 for details regarding the spectral analysis. Regions affected by telluric features are marked with encircled crosses. The spectra are shown prior to the host-light correction.

our MOSFIRE data (e.g., Denney et al. 2009; **?**). Specifically, the study of Denney et al. (2009) suggests that the use FWHM(Hβ) may introduce biases in the estimation of $M_{\rm BH}$ of up to $\sim$0.1 dex, when fitting spectra with S/N $\sim 5-10$, compared to about -0.15 dex for σ(Hβ). On the other hand, the measurement of FWHM(Hβ) is more sensitive to the accurate removal of the narrow-line emission, with an associated mass bias of as much as an order of magnitude (in the sense of significantly underestimating $M_{\rm BH}$), compared to < 0.2 dex for σ(Hβ). We therefore stress again that our linewidth measurements were performed for the best-fit profile of the *broad* component of Hβ, excluding the narrow-line emission, which is fitted with a separate component. We also note that for one of the sources, LID-496, a significant fraction of the red wing of the Hα profile is located outside of the observed spectral range. To test the robustness of our fitting procedure in this case, we used a modified version of the spectrum of LID-504 that excludes the data beyond the same (rest-frame) wavelength.[20] The spectral parameters obtained from the simulated spectrum are in excellent agreement with those derived for the full spectrum, with differences of about 0.02, 0.02, and 0.05 dex, for FWHM(Hα), $L_{\rm H\alpha}$, and L_{6200}, respectively. We are therefore confident that our best-fit emission line properties are robust, within the measurement uncertainties. The best-fit models are shown in Figures 2 and 3.

We derived measurement-related uncertainties on the best-fit Balmer line properties using a resampling approach. For each of the spectra, we generated a series of 100 realizations of the data, each of which differed from the observed spectral data by a random, normally distributed offset, determined from the error spectrum of that source. Each of these realizations was modeled using the aforementioned line fitting procedures, and the relevant quantities were recorded. Thanks to the high-quality MOSFIRE data, we obtain relatively small measurement-related uncertainties on the quantities of interest (luminosities and linewidths). The typical uncertainty on L_{5100} (among the $z \simeq 3.3$ sources) is below 0.05 dex, which is smaller than the uncertainty imposed by the flux calibration. The typical uncertainty of the broad-line FWHM is a few hundred km s^{-1}. When combining these quantities to derive "virial" mass estimators, the resulting uncertainties are of order 0.1 dex, which is smaller than the systematic uncertainties (see details in Section 2.5).

[20] We chose to use the spectrum of LID-504 since it has a similar S/N to that of LID-496, was observed within the same MOSFIRE mask, and is the next-faintest $z \simeq 2.4$ source in our sample.

2.5. *Derivation of $L_{\rm bol}$, $M_{\rm BH}$ and $L/L_{\rm Edd}$*

The bolometric luminosities of the sources, $L_{\rm bol}$, were estimated in several different ways. First, for consistency with previous studies of high-redshift unobscured AGNs with $M_{\rm BH}$ estimates, we applied bolometric corrections that translate the optical continuum and Hα line luminosities to bolometric luminosities (i.e., $f_{\rm bol}$). For $f_{\rm bol}\left(5100\text{Å}\right)$, we used the luminosity-dependent prescription described in Trakhtenbrot & Netzer (2012), which in turn relies on the *B*-band bolometric corrections presented in Marconi et al. (2004), and translated to 5100 Å assuming a UV–optical SED with $f_\nu \propto \nu^{-1/2}$ (Vanden Berk et al. 2001). In the relevant range of L_{5100}, these corrections can be described by

$$f_{\rm bol}\left(5100\text{Å}\right) = 6.58 - 0.89\mathscr{L}_{5100,45} + 0.22\mathscr{L}^2_{5100,45}, \quad (1)$$

TABLE 2
REDSHIFTS AND MULTI-WAVELENGTH LUMINOSITIES

Subsample	Object ID	z	$z_{\rm NIR}$[a]	log L_{1450}[b] (erg s^{-1})	M_{1450}[c]	log L_{2-10}[d] (erg s^{-1})	log L_{5100}[e] (erg s^{-1})	$f_{\rm AGN,5100}$[f]	log $L_{\rm bol}$ (erg s^{-1})[g] opt.	X-ray
$z\simeq3.3$	CID-349	3.5150	3.5017	45.43	-23.69	44.44 ± 0.07	$45.11^{+0.006}_{-0.008}$	0.72	45.79	46.11
	CID-413	3.3450	3.3504	45.06	-22.77	44.53 ± 0.06	$45.38^{+0.008}_{-0.009}$	0.58	45.96	46.23
	CID-113	3.3330	3.3496	46.08	-25.33	44.64 ± 0.05	$45.71^{+0.004}_{-0.004}$	1.00	46.49	46.37
	CID-947	3.3280	3.3279	45.91	-24.90	43.86 ± 0.16	$45.55^{+0.009}_{-0.009}$	0.86	46.34	45.35
	LID-775	3.6260	3.6193	45.64	-24.23	44.65 ± 0.06	$45.10^{+0.037}_{-0.047}$	0.67	45.75	46.40
	LID-1638	3.5030	3.4827	45.75	-24.49	44.47 ± 0.07	$45.77^{+0.013}_{-0.008}$	0.77	46.44	46.15
	LID-205	3.3560	3.3552	45.62	-24.17	44.75 ± 0.04	$45.15^{+0.012}_{-0.028}$	0.65	45.78	46.53
	LID-499	3.3020	3.3114	44.91	-22.41	44.47 ± 0.08	$45.49^{+0.017}_{-0.022}$	0.71	46.14	46.15
	LID-460	3.1430	3.1401	44.90	-22.38	44.99 ± 0.03	$45.37^{+0.003}_{-0.007}$	0.64	45.98	46.84
	LID-721	3.1080	3.0959	46.11	-25.40	44.53 ± 0.04	$45.58^{+0.010}_{-0.005}$	0.66	46.20	46.23
							log L_{6200}	$f_{\rm AGN,6200}$	($L_{\rm H\alpha}$)	
$z\simeq2.4$	LID-496	2.6300	2.6360	45.84	-24.71	44.29 ± 0.08	$44.82^{+0.006}_{-0.004}$	1.00	45.66	45.91
	LID-504	2.2220	2.2191	45.24	-23.22	44.95 ± 0.05	$44.59^{+0.030}_{-0.029}$	0.73	45.71	46.79
	LID-451	2.1220	2.1367	45.67	-24.30	44.61 ± 0.04	$44.93^{+0.004}_{-0.002}$	0.97	45.81	46.33
	CID-352	2.4978	2.4993	46.13	-25.44	44.88 ± 0.03	$44.99^{+0.004}_{-0.003}$	1.00	45.89	46.70

[a] Redshift measured from the best-fit model of the [O III] or (narrow) Hα lines.
[b] Monochromatic luminosity at rest-wavelength 1450Å, obtained from the optical spectra (see Table 1).
[c] Absolute magnitude at 1450Å, following $M_{1450}=-2.5\log L_{1450}+89.9$.
[d] *Chandra*-based, obscuration-corrected rest-frame hard-band [$(2-10)$ keV] luminosity, taken from Marchesi et al. (2015).
[e] Monochromatic luminosities at rest-wavelength 5100 Å (for $z\simeq3.3$ AGNs) or 6200Å (for $z\simeq2.4$ AGNs), *uncorrected* for host contamination. The tabulated errors reflect only measurement-related uncertainties.
[f] AGN luminosity fraction at $\lambda_{\rm rest}=5100$ or 6200Å, determined from SED decomposition.
[g] Bolometric luminosity estimates based either on L_{5100} (or $L_{\rm H\alpha}$) or on L_{2-10}.

where $\mathscr{L}_{5100,45}\equiv\log\left(L_{5100}/10^{45}\,{\rm erg\,s^{-1}}\right)$. For the $z\simeq2.4$ objects, we used the $L_{\rm H\alpha}$-dependent bolometric corrections suggested in Greene & Ho (2007), which provide

$$L_{\rm bol}\left(L_{\rm H\alpha}\right)=2.34\times10^{44}\left(\frac{L_{\rm H\alpha}}{10^{42}\,{\rm erg\,s^{-1}}}\right)^{0.86}. \quad (2)$$

This $L_{\rm H\alpha}$-based prescription was calibrated against L_{5100} for a sample of low-redshift AGNs, assuming $f_{\rm bol}\left(5100{\rm \AA}\right)=9.8$. To test the consistency of these $L_{\rm H\alpha}$-based estimates of bolometric luminosity, we translated the observed continuum luminosities at 6200 Å (Table 2) to L_{5100} (assuming $f_\nu\propto\nu^{-1/2}$) and then used Equation 1 to obtain another set of $L_{\rm bol}$ estimates for the four $z\simeq2.4$ sources. These latter L_{6200}-based estimates of $L_{\rm bol}$ are consistent with those derived directly from Equation 2, with a (median) offset of merely 0.03 dex. The bolometric luminosities obtained through Equations 1 and 2 are in the range of $L_{\rm bol}\simeq(6-31)\times10^{45}\,{\rm erg\,s^{-1}}$. Second, we used the X-ray luminosities measured from the *Chandra* data, and X-ray bolometric corrections. For $f_{\rm bol}\left(L_{2-10}\right)$, we used the prescription of Marconi et al. (2004), for consistency with other studies using the *Chandra* survey data. These *Chandra*-based $L_{\rm bol}$ values are in the range $L_{\rm bol}\left(L_{2-10},Chandra\right)=(2-68)\times10^{45}\,{\rm erg\,s^{-1}}$. Since the *XMM*-based estimates of L_{2-10} are highly consistent with the *Chandra* ones, they result in similar X-ray-based $L_{\rm bol}$ estimates. Finally, we note that yet another set of $L_{\rm bol}$ estimates for nine of our sources (six of those at $z\simeq3.3$) is available from the multi-wavelength analysis performed for our sources as part of the *XMM*-COSMOS survey by Lusso et al. (2010, see also Lusso et al. 2011). Unlike the previous $L_{\rm bol}$ estimates discussed here, these were obtained by integrating the multi-wavelength AGN SEDs up to 1 μm (and further fixing the unobserved FUV and hard X-ray parts of the SED). These *XMM*- and SED-based $L_{\rm bol}$ estimates are in the range $L_{\rm bol}\left({\rm SED},XMM\right)=(1-41)\times10^{45}\,{\rm erg\,s^{-1}}$, and in good agreement with our estimates of $L_{\rm bol}$ based on L_{5100} or $L_{\rm H\alpha}$ – the median offset is 0.09 dex (0.03 dex for the $z\simeq3.3$ AGNs; *XMM*- and SED-based $L_{\rm bol}$ estimates are higher), and the scatter is 0.37 dex (0.17 dex for $z\simeq3.3$ AGNs).

In Table 2 we list the different bolometric luminosities we obtained for our sources. The L_{2-10}-based estimates of $L_{\rm bol}$ for our sources are generally consistent with those derived from L_{5100} and $L_{\rm H\alpha}$, with a median offset of about 0.07 dex between the latter and the former, and virtually all the sources having differences within 0.5 dex. The extreme source CID-947 is exceptionally weak in the X-rays, resulting in an $L_{\rm bol}$ difference of almost an order of magnitude. Moreover, as noted in T15, the X-ray luminosity of this broad-absorption-line quasar as derived from the *XMM*-COSMOS survey is significantly higher than that obtained from the *Chandra* data, which might be related to varying obscuration along the line of sight. In what follows, we chose to use the bolometric luminosities based on L_{5100} and $L_{\rm H\alpha}$, given the (generally) higher quality of the rest-frame optical data, the limited availability of other $L_{\rm bol}$ estimates (i.e., *XMM*+SED), and in order to be consistent with previous studies of $z>2$ unobscured AGNs (see the comparison samples in Section 3.2).

We estimated black hole masses for the sources using the quantities derived from the best-fitting spectral models, and following the prescription used in several recent works (Netzer et al. 2007; Trakhtenbrot & Netzer 2012). For the $z\simeq3.3$ sources, we correct the continuum luminosities to account for the emission from the stellar component in the host galaxies. These scaling corrections are derived from the spectral compositions of the broad-band SEDs of the sources, which are described in detail in a forthcoming publication. In short, the stellar component is modeled using a large grid of (single)

stellar population models, with a broad range of ages, star formation histories, and dust extinction. We use the stellar template that provides the best fit to the SED, provided that the UV-optical regime of all SEDs is AGN-dominated. The scaling factors thus computed, which are simply the fraction of AGN-related emission at $\lambda_{\rm rest} = 5100$ Å, are in the range of $f_{\rm AGN}\left(5100\text{Å}\right) \sim 0.55-1$. Next, H$\beta$-based BH masses are estimated using the expression

$$M_{\rm BH}\left({\rm H}\beta\right) = 1.05\times10^{8}\left(\frac{L_{5100}}{10^{46}\,{\rm erg\,s^{-1}}}\right)^{0.65} \times\left[\frac{\rm FWHM\left({\rm H}\beta\right)}{10^{3}\,{\rm km\,s^{-1}}}\right]^{2} M_{\odot}\,. \quad (3)$$

This prescription is based on the $R_{\rm BLR}-L_{5100}$ relation obtained through reverberation mapping of low-redshift sources with comparable (optical) luminosities (Kaspi et al. 2005), and assumes a BLR "virial factor" of $f = 1$ (see also Onken et al. 2004; Woo et al. 2010; Grier et al. 2013). The exponent of the luminosity term means that the aforementioned host-light corrections affect the derived masses by at most ∼0.17 dex. We verified that using alternative $R_{\rm BLR}$ estimators would not significantly affect our determinations of $M_{\rm BH}$. In particular, in the range of optical luminosities of our sources, the $R_{\rm BLR}-L_{5100}$ relation of Bentz et al. (2013) results in BLR sizes (and therefore BH masses) that are systematically *smaller* than those derived by the relation of Kaspi et al. (2005). The difference between the two $R_{\rm BLR}$ estimates increases with increasing L_{5100} (or $M_{\rm BH}$), but for our sources it remains very small, in the range 0.02-0.1 dex (median value 0.06 dex).

For the sources at $z \simeq 2.4$ we estimated $M_{\rm BH}$ from the luminosity and width of the Hα line, following the prescription of Greene & Ho (2005):

$$M_{\rm BH}\left({\rm H}\alpha\right) = 1.3\times10^{6}\left(\frac{L_{\rm H\alpha}}{10^{42}\,{\rm erg\,s^{-1}}}\right)^{0.57} \times\left[\frac{\rm FWHM\left({\rm H}\alpha\right)}{10^{3}\,{\rm km\,s^{-1}}}\right]^{2.06} M_{\odot}\,. \quad (4)$$

This $M_{\rm BH}$ was derived through an empirical secondary calibration against Hβ-related quantities (L_{5100} and FWHM[Hβ]).[21] These two prescriptions were also used to derive masses for each of the spectra simulated within our resampling scheme, thus providing measurement-related uncertainties on the $M_{\rm BH}$ estimates.

We note that the relevant luminosities of our sources are well within the range of the reverberation mapping campaigns that stand at the base of "virial" estimates of $M_{\rm BH}$. In particular, our $z \simeq 3.3$ sources have (host-corrected) optical luminosities comparable with those of low-redshift PG quasars, for which $R_{\rm BLR}$ estimates were obtained in several reverberation mapping studies (e.g., Kaspi et al. 2000, 2005; Vestergaard & Peterson 2006). Thus, our virial estimates of $M_{\rm BH}$ do not require the extrapolation of the $L_{5100}-R_{\rm BLR}$ relation toward extremely high luminosities, which is often the case in other studies of $z \gtrsim 2$ AGNs (e.g., Shemmer et al. 2004; Marziani et al. 2009).

[21] Thus, the luminosity-term exponent (0.57) is not directly observed in an $R_{\rm BLR}-L_{\rm H\alpha}$ relation, and the velocity-term exponent (2.06) is not strictly virial.

The $M_{\rm BH}$ and $L_{\rm bol}$ estimates were finally combined to obtain Eddington ratios, $L/L_{\rm Edd} \equiv L_{\rm bol}/\left(1.5\times10^{38}M_{\rm BH}/M_{\odot}\right)$ (suitable for solar-metalicity gas). As mentioned above, we choose to use the L_{5100}-based estimates of $L_{\rm bol}$. Choosing instead the L_{2-10}-based estimates would lead to slightly higher values of $L/L_{\rm Edd}$. Such a choice would not significantly affect any of our main findings, and would actually strengthen our claim of a lack of low-$L/L_{\rm Edd}$ and high-$M_{\rm BH}$ AGNs (see Section 3.2). Our estimates of $M_{\rm BH}$ and $L/L_{\rm Edd}$ are listed in Table 3. Since the measurement-related uncertainties on $M_{\rm BH}$ are relatively small, rarely exceeding 0.1 dex, the real uncertainties on $M_{\rm BH}$ are dominated by the systematics associated with the "virial" mass estimators we used. These are estimated to be of order ∼0.3 dex for the $z \simeq 3.3$ sources (e.g., Shen 2013), and yet higher for the $z \simeq 2.4$ ones, as their mass estimator is based on a secondary calibration of $M_{\rm BH}\left({\rm H}\alpha\right)$.

3. RESULTS AND DISCUSSION

We next discuss the main results of the detailed analysis of the Balmer emission line complexes. We first highlight a few objects with peculiar emission line properties, before addressing the implications of our measurements for the observed early evolution of SMBHs.

3.1. *Emission Line Properties*

Two of the $z \simeq 3.3$ sources, LID-205 and LID-721, have extremely weak or indeed undetectable broad Hβ emission lines. Our fitting procedure suggests that the rest-frame equivalent widths of these components are approximately EW$\left({\rm H}\beta\right) \simeq 10-15$ Å. More importantly, a series of (manual) fitting attempts demonstrated that the data can be adequately modeled without *any* broad Hβ components. We also verified that these low EW(Hβ) values are not due to measurement-related uncertainties. For LID-205, 90% (99%) of the resampling simulations resulted in EW$\left({\rm H}\beta\right) < 18$ Å (30 Å, respectively). For LID-721, the corresponding quantiles are EW$\left({\rm H}\beta\right) < 20$ and 25 Å, respectively. The best-fit values are lower, by at least a factor of 4, than the median value of EW(Hβ) we find for the rest of the $z \simeq 3.3$ sources. Moreover, such weak Hβ lines are not observed at all within other samples of $z \gtrsim 2$ AGNs (Shemmer et al. 2004; Netzer et al. 2007; Marziani et al. 2009), where the weakest lines have EW$\left({\rm H}\beta\right) \sim 40$Å, and the median values are above ~ 75Å. Another $z \simeq 3.3$ source, CID-413, has a relatively weak broad Hβ line, with EW$\left({\rm H}\beta\right) = 31$ Å. Our simulations, however, show that the Hβ emission can be accounted for with significantly stronger components, reaching EW$\left({\rm H}\beta\right) \simeq 70$ Å. Indeed, this ambiguity regarding the broad component of CID-413 is reflected in the atypically large uncertainties on FWHM(Hβ) and $M_{\rm BH}$ (see Table 3). We chose, however, to include this source in the analysis that follows, since even the most extreme realizations present EW$\left({\rm H}\beta\right) > 25$ Å.

We stress that the two "Hβ-weak" sources we identified have strong and unambiguous [O III] emission lines, with flux ratios $\left[{\rm O\,III}\right]/{\rm H}\beta \gg 3$, further supporting the identification of the sources as emission line systems dominated by an AGN ionization field (e.g., Baldwin et al. 1981; Kewley et al. 2006). We verified that the observed-frame optical, rest-frame UV zCOSMOS and IMACS spectra of the two Hβ-weak AGNs present broad and strong high-ionization C IV λ1549 emission lines. Indeed, the C IV lines have EW$\left({\rm C\,IV}\right) = 118$ and 57 Å (for LID-205 and LID-721, respectively). This, as well

TABLE 3
SPECTRAL MEASUREMENTS AND DERIVED SMBH PROPERTIES

sub-sample	Object ID	$\log L_{H\beta}$ (erg s^{-1})	FWHM(Hβ) (km s^{-1})	$\log M_{BH}$ ($M_\odot$)	$\log L/L_{Edd}$ [a]	$\dot{M}_{AD}$ ($M_\odot$ yr^{-1}) [b] L_{bol}	AD	t_{growth} (Gyr) [c] L/L_{Edd}	$\dot{M}$
$z \simeq 3.3$	CID-349	43.14	3223^{+592}_{-385}	$8.37^{+0.13}_{-0.11}$	-0.76	1.08	1.29	0.25	0.20
	CID-413	42.85	4149^{+1707}_{-1143}	$8.70^{+0.18}_{-0.25}$	-0.92	1.60	1.11	0.37	0.51
	CID-113	43.80	2959^{+101}_{-117}	$8.78^{+0.03}_{-0.03}$	-0.46	5.51	6.54	0.13	0.10
	CID-947	43.52	11330^{+929}_{-799}	$9.84^{+0.07}_{-0.06}$	-1.67	3.03	0.22	2.09	34.68
	LID-775	43.40	4700^{+450}_{-328}	$8.67^{+0.10}_{-0.06}$	-1.10	0.99	0.56	0.55	0.92
	LID-1638	43.67	4071^{+316}_{-308}	$9.02^{+0.06}_{-0.07}$	-0.75	4.86	3.09	0.25	0.37
	LID-499	43.54	3451^{+606}_{-360}	$8.67^{+0.15}_{-0.10}$	-0.70	2.43	2.32	0.23	0.22
	LID-460	43.52	2260^{+45}_{-89}	$8.19^{+0.02}_{-0.05}$	-0.39	1.70	3.94	0.11	0.04
		$\log L_{H\alpha}$	FWHM(Hα)						
$z \simeq 2.4$	LID-496	43.50	3533^{+53}_{-39}	$8.10^{+0.02}_{-0.01}$	-0.61	0.81	2.15	0.18	0.07
	LID-504	43.56	3401^{+148}_{-100}	$8.10^{+0.06}_{-0.05}$	-0.56	0.91	0.59	0.16	0.24
	LID-451	43.67	3278^{+71}_{-139}	$8.13^{+0.01}_{-0.06}$	-0.50	1.14	2.75	0.14	0.05
	CID-352	43.77	3261^{+236}_{-279}	$8.18^{+0.06}_{-0.07}$	-0.46	1.38	3.13	0.13	0.05

[a] Based on L_{bol} estimated from L_{5100} (or $L_{H\alpha}$).
[b] Accretion rate estimates based on either L_{bol} (and $\eta = 0.1$), or an accretion disk model Equation 5 ("AD").
[c] Based on either L/L_{Edd} (via Equation 6) or on $\dot{M}_{AD}$, and further assumes $\eta = 0.1$.

as the strong [O III] lines, suggests that the low EWs of Hβ are *not* due to attenuation by dust along the line of sight. Furthermore, the ratio of UV to optical luminosities of the Hβ weak AGNs, $L_{1450}/L_{5100} \simeq 3$, is consistent with what is found in large samples of normal AGNs (e.g., Trakhtenbrot & Netzer 2012), suggesting that the broad Hβ lines in these two sources are emphnot diluted by stellar emission from the host. We also note that the broad Hβ lines in these sources are significantly weaker than those detected in the spectra of "weak line quasars", which are defined based on their weak UV lines (i.e., Lyα + N V, or C IV; see, e.g., Shemmer et al. 2010; Plotkin et al. 2015, and references therein). One intriguing explanation may be that the Hβ-weak AGNs have experienced a dramatic decrease in the emission of ionizing radiation since the optical spectra were taken, i.e. on a roughly year-long timescale (in the AGN reference frames). This change may have driven a sharp decrease in the BLR emission, but has yet to reach the more extended NLR, which would explain the strong [O III] emission. Such a drastic decrease in ionizing flux should, however, manifest itself also as a decrease in (rest-frame) optical continuum luminosity, which is not observed (see the comparison of K-band fluxes in Table 1). In this sense, our Hβ-weak AGNs are inconsistent with the growing number of "changing-look" AGNs, detected through dramatic drops in both UV-optical continuum *and* BLR emission (see, e.g., recent studies by Denney et al. 2014; LaMassa et al. 2015; Runnoe et al. 2016, and references therein). In any case, revisiting these sources with optical spectroscopy may test this explanation and clarify the situation. We therefore conclude that our sample contains two sources (about 12.5% of the sample) with abnormally weak broad Hβ lines, which are not due to the lack of gas in the BLR.

The spectrum of one other $z \simeq 3.3$ source, LID-1638, presents an abnormally broad [O III] emission feature. A manual inspection of the data provides a rough estimate of FWHM $\sim 3000\,\mathrm{km\,s^{-1}}$ for the width of this feature. At these large widths, the feature is basically a combination of the two different [O III] emission lines (with some additional, minor contribution from Fe II). This width appears to be comparable to that of the adjacent Hβ line, which otherwise appears rather normal. Such broad [O III] emission features are rarely reported in large samples of lower-redshift AGNs (e.g., Boroson & Green 1992; Shen et al. 2011; Trakhtenbrot & Netzer 2012), but may be related to prominent blue wings (e.g., Komossa et al. 2008).[22] Another explanation is that the [O III] profile consists of two separate narrow lines, emitted from separate NLRs, as observed in dual AGN candidates (e.g., Comerford et al. 2012, and references therein). In any case, a detailed analysis and interpretation of the peculiar [O III] profile are beyond the scope of the present study, as we focus on the broad Hβ component. To account for the broadened [O III] emission, we refitted the spectrum of this source with a modified constraint of FWHM $\leq 3000\,\mathrm{km\,s^{-1}}$ for the narrow emission features (both [O III] and Hβ). The FWHM(Hβ) resulting from this, of about 4100 km s^{-1}, is highly consistent with the value obtained with the "standard" line fitting procedure. Removing the width constraint altogether results in yet broader [O III] features, exceeding 5000 km s^{-1}, but with FWHM(Hβ) decreasing to $\sim 3700\,\mathrm{km\,s^{-1}}$. This is mainly due to the fact that the fitting procedure does not allow for a significant (broader than usual) narrow component for Hβ. However, we find the overall fit to the data in this case unsatisfactory, and note that in any case this would result in a decrease of merely 0.1 dex in M_{BH}. The best-fit parameters tabulated for LID-1638 in Table 3 are therefore those obtained with the constraint FWHM [O III] $\leq 3000\,\mathrm{km\,s^{-1}}$.

3.2. *Trends in M_{BH} and L/L_{Edd} at $z > 2$*

Figure 4 presents the distributions of relevant apparent brightness and estimates of L_{bol}, M_{BH}, and L/L_{Edd} for the sources studied here, as a function of redshift, in the context of other samples of optically selected and unobscured AGNs at $z > 2$, for which these quantities were reliably determined. The relevant samples are those presented by Shemmer et al. (2004) and Netzer et al. (2007, at $z \simeq 3.3$ and 2.4); by Trakhtenbrot et al. (2011, $z \simeq 4.8$); and by Kurk et al. (2007) and

[22] The automated procedures used for very large surveys (e.g., SDSS) are restricted to FWHM $\simeq 1000\,\mathrm{km\,s^{-1}}$ and obviously lack a manual inspection of the (tens of thousands of) spectra.

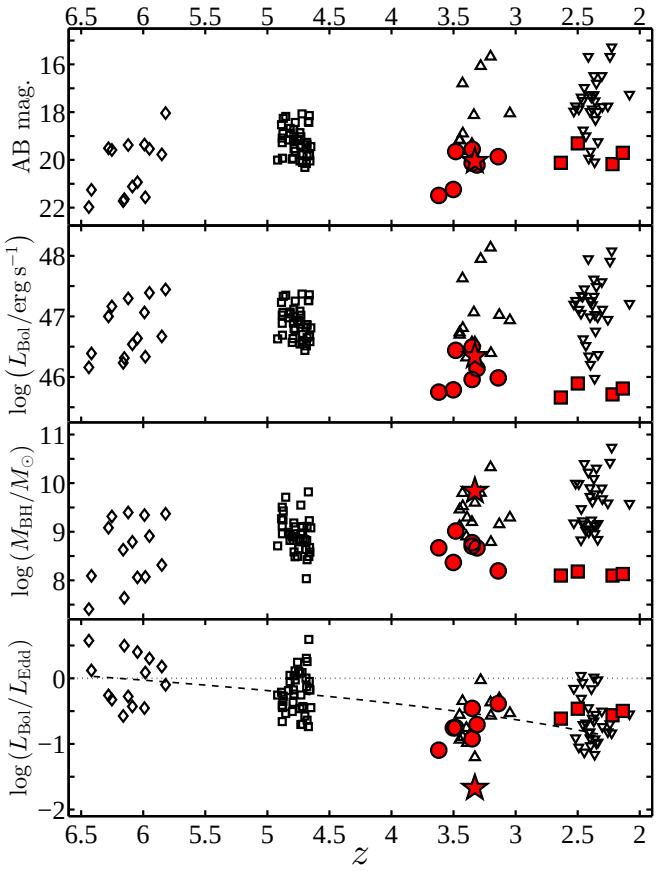


FIG. 4.— From top to bottom, trends of observed (NIR) brightness, $L_{\rm bol}$, $M_{\rm BH}$, and $L/L_{\rm Edd}$ for the available samples of unobscured AGNs at $z > 2$, with reliable determinations of $M_{\rm BH}$. The red symbols represent the measurements reported in this work, at $z \simeq 3.3$ and 2.4 (circles and squares, respectively). CID-947, which was analyzed in detail in Trakhtenbrot et al. (2015), is highlighted by a star. The different black symbols represent other, optically selected sources, studied in the combined sample of Shemmer et al. (2004) and Netzer et al. (2007, triangles at $z \simeq 2.4$ and $\simeq 3.3$); Trakhtenbrot et al. (2011, squares at $z \simeq 4.8$); and the combined samples of Kurk et al. (2007) and Willott et al. (2010, diamonds at $z \simeq 6.2$). The dotted line in the bottom panel marks the Eddington limit, i.e., $L/L_{\rm Edd} = 1$. The dashed line follows $L/L_{\rm Edd} \propto (1+z)^2$, reaching $L/L_{\rm Edd} = 1$ at $z = 6.2$, which represents the general trend among the samples considered here.

Willott et al. (2010, $z \simeq 6.2$). The apparent magnitudes in the top panel of the diagram represent the NIR bands at which either the Hβ ($z \simeq 2.4$ and $\simeq 3.3$) or Mg II broad emission lines would be observed, which is the H-band for $z \simeq 2.4$ and 4.8 sources or the K-band for $z \simeq 2.4$ and 6.2 sources.[23] The Hβ-based $M_{\rm BH}$ estimates for all the $z \simeq 2.4$ and $\simeq 3.3$ AGNs in these comparison samples are based on the same prescription as we use here (Equation 3). For consistency with previous studies (and in particular with Trakhtenbrot et al. 2011), the Mg II-based $M_{\rm BH}$ estimates for $z > 4.5$ sources are based on the calibration of McLure & Dunlop (2004). The bolometric corrections for all the comparison sources are based on the same procedure as the one used here (Equation 1), extended to $f_{\rm bol}\,(3000\text{Å})$ for $z > 4.5$ sources (see Trakhtenbrot & Netzer 2012). We note that several other studies have provided (relatively small) samples with $M_{\rm BH}$ estimates for AGNs at $2 \lesssim z \lesssim 3$ (e.g., Alexander et al. 2008; Dietrich et al. 2009; Marziani et al. 2009; Bongiorno et al. 2014; Banerji et al. 2015; Glikman et al. 2015; Suh et al. 2015). Likewise, there are several additional $z > 5$ quasars with Mg II-based $M_{\rm BH}$ estimates (e.g., De Rosa et al. 2011, 2014; Wang et al. 2015; Wu et al. 2015). However, we chose not to include these in our comparative analysis, because of our choice to focus on $z > 3$ systems, the small sizes of the samples, and the inhomogeneity the methods of target selection and analysis used in these studies. We instead focus on the largest samples of unobscured AGNs at $z > 3$, selected on the basis of rest-frame UV properties, and for which $M_{\rm BH}$ estimates were derived through an homogeneous spectral analysis.

As Figure 4 shows, the lower luminosities of the sources studied here are mainly driven by BH masses that are lower than those found for the more luminous $z \simeq 3.3$ sources analyzed in previous studies, while their accretion rates actually overlap. For example, about 85% of the objects in the combined sample of Shemmer et al. (2004) and Netzer et al. (2007) have $M_{\rm BH} > 8 \times 10^8\,M_\odot$, while about 85% of the AGNs studied here (save CID-947) have a mass that is lower than this. The median $M_{\rm BH}$ of our $z \simeq 3.3$ AGNs, $\sim 5 \times 10^8\,M_\odot$, is lower than that of the previously studied sources ($2.4 \times 10^9\,M_\odot$) by about 0.7 dex. On the other hand, the accretion rates of our AGNs – which span the range $L/L_{\rm Edd} \sim 0.1 - 0.5$ – are similar to those found for the more luminous quasars, and also to those of (optically selected) SDSS quasars at $z \sim 0.5 - 1$ (Trakhtenbrot & Netzer 2012; Schulze et al. 2015). The obvious outlier in all these comparisons is CID-947, which has $M_{\rm BH}$ comparable to the most massive SMBHs at $z > 2$, and an extremely low accretion rate, of merely $L/L_{\rm Edd} \simeq 0.02$. The four $z \simeq 2.4$ AGNs are powered by yet smaller SMBHs, with typical (median) masses of $M_{\rm BH} \simeq 1.3 \times 10^8\,M_\odot$, accreting at normalized rates of $L/L_{\rm Edd} \simeq 0.3$. These masses are lower, by about an order of magnitude, than those of the faintest AGNs in the combined $z \simeq 2.4$ sample of Shemmer et al. (2004) and Netzer et al. (2007, i.e., those AGNs with $L_{\rm bol} \lesssim 3 \times 10^{46}\,{\rm erg\,s^{-1}}$).

As mentioned in Section 2.1, our chosen flux limit for the $z \simeq 3.3$ AGNs means we could have recovered sources with masses as low as $M_{\rm BH} \sim 7 \times 10^7\,M_\odot$ or with accretion rates as low as $L/L_{\rm Edd} \sim 0.01$. However, as Figure 4 demonstrates, the majority of $z \simeq 3.3$ sources in our sample do not reach these lower limits. The accretion rates we find ($0.1 \lesssim L/L_{\rm Edd} \lesssim 0.5$) are about an order of magnitude above the estimated survey limit. Given the flux limit of the sample, objects with $L/L_{\rm Edd} \simeq 0.01$ should have $M_{\rm BH} \simeq 5 \times 10^9\,M_\odot$ in order to be included in our study. Indeed, the only object with $L/L_{\rm Edd} < 0.1$ is, again, the extremely massive source CID-947, which reaches $L/L_{\rm Edd} \simeq 0.02$. This low value, as well as other, indirect evidence, indicates that this source is most probably observed at the final stages of SMBH growth, after accreting at much higher rates at yet higher redshifts. Several previous studies of the distributions of $L/L_{\rm Edd}$ did identify significant populations of intermediate-redshift AGNs ($1 < z < 2$) with $0.01 < L/L_{\rm Edd} < 0.1$ (e.g., Gavignaud et al. 2008; Trump et al. 2009a; Trakhtenbrot & Netzer 2012; Schulze et al. 2015). Specifically, the low-$L/L_{\rm Edd}$ AGNs studied in Trump et al. (2009a) and Schulze et al. (2015) have BH masses comparable to those studied here. We conclude that our sample presents compelling evidence for the lack of high-mass, slowly accreting SMBHs - with $M_{\rm BH} \gtrsim 2 \times 10^9\,M_\odot$ and

[23] Note that for our $z \simeq 2.4$ COSMOS AGNs we use the H-band magnitudes (from UltraVISTA McCracken et al. 2012), although we study the Hα line in the K band. The magnitudes for the other sources were compiled from the original studies, where the K-band magnitudes of the $z \simeq 6.2$ sources were estimated from the published J-band magnitudes (Jiang et al. 2006), and assuming $J_{\rm Vega} - K_{\rm Vega} = 1.25$ and $H_{\rm Vega} - K_{\rm Vega} = 0.75$.

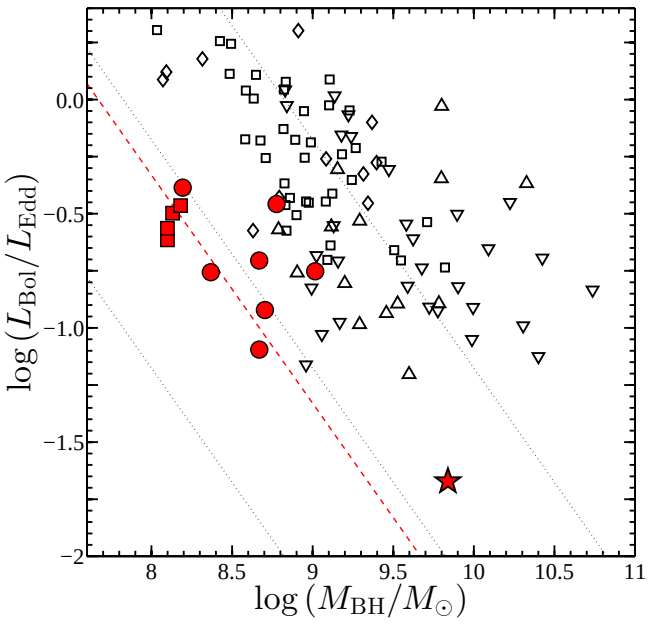


FIG. 5.— Accretion rate, in terms of $L/L_{\rm Edd}$, vs. black hole mass, $M_{\rm BH}$, for the sources studied here and several other relevant samples of high-redshift AGNs. The symbols are identical to those in Figure 4). The dotted lines represent constant bolometric luminosities of $L_{\rm bol} = 10^{45}$, 10^{46}, and $10^{47}\,{\rm erg\,s^{-1}}$. The red dashed line represents the flux limit of our study, $L_{\rm bol} = 7.8\times10^{45}\,{\rm erg\,s^{-1}}$ (at $z = 3.5$; see Section 2.1), which is most relevant for the $z \simeq 3.3$ sources. Some of the $z \simeq 3.3$ AGN fall below the flux limit, due to the host-light corrections. Compared to the combined sample of Shemmer et al. (2004) and Netzer et al. (2007), our sources exhibit lower masses but comparable accretion rates. With the exception of the extreme source CID-947 (red star), our sample lacks AGNs with high $M_{\rm BH}$ and low $L/L_{\rm Edd}$ (i.e., $M_{\rm BH} > 2\times10^9\,M_\odot$ and $L/L_{\rm Edd} < 0.1$).

$L/L_{\rm Edd} \lesssim 0.1$. Such sources would "fill the gap" between most of the $z \simeq 3.3$ sources and CID-947 in Figure 5. However, larger samples are needed to establish this conclusion more firmly.

3.3. *Physical Accretion Rates*

Given reliable estimates of $M_{\rm BH}$, and further assuming that the accretion onto the SMBHs occurs within a thin accretion disk, one can derive prescriptions for the estimation of the *physical* accretion rate (i.e., in $M_\odot\,{\rm yr^{-1}}$) through the accretion disk, $\dot{M}_{\rm AD}$. Several studies derived such prescriptions based on the classical accretion disk model of (Shakura & Sunyaev 1973, e.g., Collin et al. 2002), or on more elaborate models that take into account additional complex processes (e.g., general relativistic effects, Comptonization, and winds; see Davis & Laor 2011; Netzer & Trakhtenbrot 2014, and references therein). Generally, such prescriptions require measurements of the (rest-frame) optical luminosity of the AGNs, which is predominantly emitted by the outer parts of the accretion disk, and is thus mostly unaffected by the spin of the SMBH.

We estimated $\dot{M}_{\rm AD}$ for the 12 AGNs with mass determinations using the prescription presented in Netzer & Trakhtenbrot (2014, see also Davis & Laor 2011):

$$\dot{M}_{\rm AD} \simeq 2.4\left(\frac{L_{5100,45}}{\cos i}\right)^{3/2} M_8^{-1}\ M_\odot\,{\rm yr^{-1}}\,, \qquad (5)$$

where $L_{5100,45} \equiv L_{5100}/10^{45}\,{\rm erg\,s^{-1}}$, $M_8 \equiv M_{\rm BH}/10^8\,M_\odot$, and $\cos i$ represents the inclination of the accretion disk with regard to the line of sight, assumed here to be $\cos i = 0.8$ (see Netzer & Trakhtenbrot 2014 for the full analytical expression and more details).

The resulting accretion rates of the $z \simeq 3.3$ AGNs are in the range of $\dot{M}_{\rm AD} \sim 0.6-6.5\,M_\odot\,{\rm yr^{-1}}$. A comparison of the $\dot{M}_{\rm AD}$ values obtained through Equation 5 and those estimated from $L_{\rm bol}$ (Table 3) suggests that, for most of the sources, the observed data are broadly consistent with a radiatively efficient accretion with $\eta \sim 0.1$, as assumed in some of the evolutionary calculations presented in this paper. However, we note that a more detailed examination reveals that the *typical* (median) radiative efficiency needed to account for the observed $L_{\rm bol}$, given the $\dot{M}_{\rm AD}$ estimates, is somewhat higher, at about $\eta \simeq 0.15$. The only outlier is CID-947 for which the two $\dot{M}_{\rm AD}$ estimates suggest a very high radiative efficiency, reaching (and formally exceeding) the maximum value allowed within the standard accretion disk theory, of $\eta \simeq 0.32$. We note that while CID-947 has an extremely low $L/L_{\rm Edd}$ ($\sim$0.02), its physical accretion rate of about $0.4\,M_\odot\,{\rm yr^{-1}}$ is low but not extreme. Two other sources (LID-775 and LID-504) have comparably low $\dot{M}_{\rm AD}$, despite the fact that their masses are lower than that of CID-947 by more than an order of magnitude. The typically high radiative efficiencies we find are in agreement with the results of several previous studies reporting similar findings for high-mass and/or high-redshift SMBHs, relying either on direct measurements of the iron Kα line (Reynolds 2014; Reynolds et al. 2014), on arguments similar to the one presented here (e.g., Davis & Laor 2011; Netzer & Trakhtenbrot 2014; Trakhtenbrot 2014), or on indirect evidence involving the AGN population as a whole (e.g., Elvis et al. 2002).

Finally, the $\dot{M}_{\rm AD}$ estimates can be used to derive an initial set of estimates of growth time for the SMBHs under study, defined as $t_{\rm growth,AD} \equiv M_{\rm BH}/\dot{M}_{\rm BH} = M_{\rm BH}/\dot{M}_{\rm AD}\,(1-\eta)$. Simply assuming $\eta = 0.1$, we derive growth times that are generally in the range of $t_{\rm growth,AD} \sim 0.1-0.85$ Gyr, again showing that most of the accretion should have happened at higher redshifts. CID-947 has an extremely long timescale of $\sim$ 23 Gyr. These timescales are generally longer, by a factor of about 1.6, than those derived from $L/L_{\rm Edd}$ alone (see Section 3.4 below).

3.4. *Early BH Growth*

Assuming a SMBH accretes matter with a constant $L/L_{\rm Edd}$ and radiative efficiency η, its mass increases exponentially with time, with a typical e-folding timescale of

$$\tau = 4\times10^8\ \frac{\eta/(1-\eta)}{L/L_{\rm Edd}}\ {\rm yr}. \qquad (6)$$

If one further assumes a certain initial (seed) BH mass, $M_{\rm seed}$, then the time required to grow from $M_{\rm seed}$ to the observed $M_{\rm BH}$, $t_{\rm growth}$, is

$$t_{\rm growth} = \tau\ \ln\left(\frac{M_{\rm BH}}{M_{\rm seed}}\right)\ {\rm yr}. \qquad (7)$$

For the $z \simeq 3.3$ AGNs studied here, the e-folding timescales are in the range $0.1-2$ Gyr, assuming $\eta = 0.1$. For the lower-redshift sources the timescales are shorter, at about 0.1 Gyr. Further assuming that $M_{\rm seed} = 100$, 10^4, or $10^6\,M_\odot$ results in growth times in the range of $1.5-8.5$, $1-6$, or $0.5-3.4$ Gyr, respectively, for the $z \simeq 3.3$ sources, excluding CID-947. The atypically low accretion rate of CID-947 translates to an e-folding timescale of 2 Gyr. Even in the most favorable scenario of $M_{\rm seed} = 10^6\,M_\odot$, the growth time is longer than the

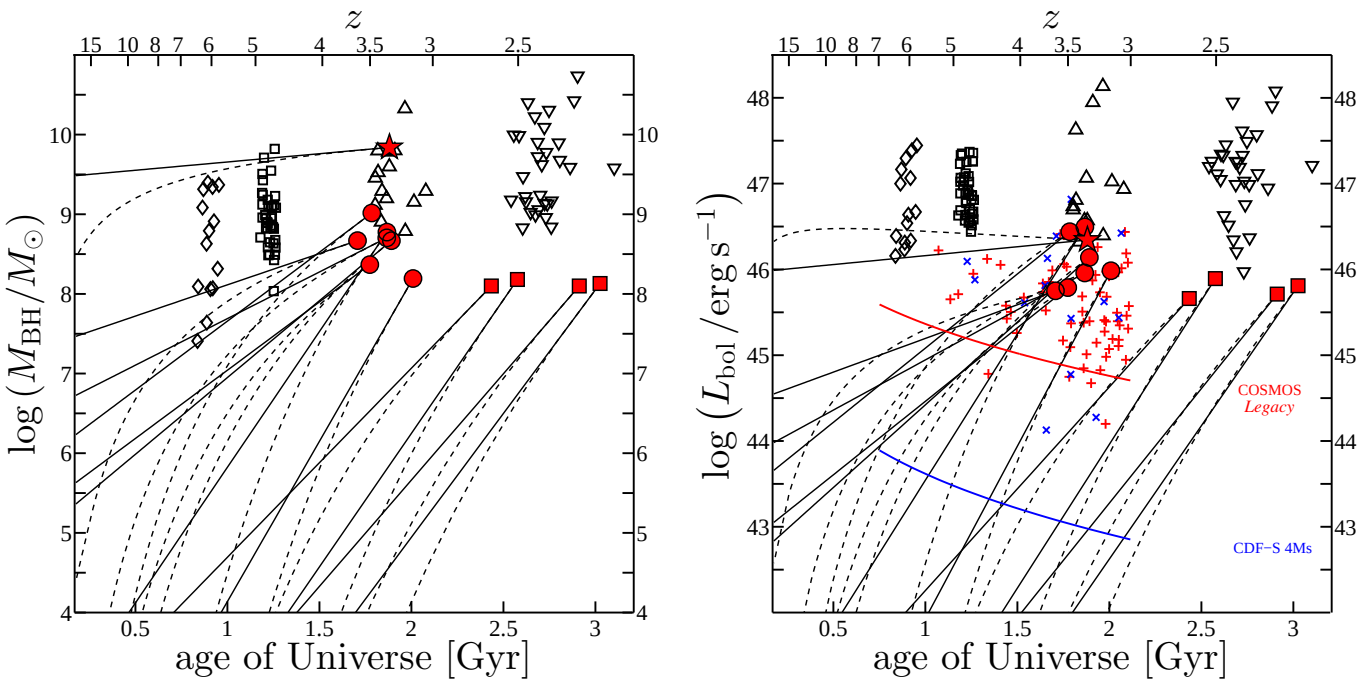


FIG. 6.— Calculated evolutionary tracks of M_{BH} and L_{bol} back to $z = 20$, for the sources studied here, compared with other relevant $z > 2$ samples (as described in Figure 4). The calculations assume continuous accretion at a (fixed) radiative efficiency of $\eta = 0.1$, and accretion rates that are either constant (at observed values), or evolve as $(1+z)^2$ (illustrated with solid and dashed lines, respectively). *Left:* evolutionary tracks of M_{BH}. Some of the $z \simeq 3.3$ sources studied here require massive seed BHs, with $M_{seed} \gtrsim 10^4 M_\odot$, and/or a higher accretion rate in previous epochs. For the extreme source CID-947, these calculation strongly support a scenario in which the SMBH used to accrete at *much* higher rates at $z \gtrsim 3.5$. The $z \simeq 2.4$ sources can be easily explained by stellar BH seeds, even if invoking a non-unity duty cycle. *Right:* evolutionary tracks of L_{bol}. Here we also plot high-z X-ray-selected samples with spectroscopic redshifts from the *Chandra COSMOS Legacy* (red "+"; M15) and the 4Ms CDF-S (blue "×"; Vito et al. 2013) surveys. The flux limits of these surveys are indicated as colored dashed lines (assuming the Marconi et al. 2004 bolometric corrections). Both surveys should, in principle, detect the progenitors of our sample of AGNs, up to $z \sim 5-6$. However, such faint AGNs are detected at very small numbers, if at all (see discussion in text).

age of the Universe (at the observed epoch), suggesting that CID-947 must have experienced a dramatic drop in L/L_{Edd} (see T15 for a detailed discussion).

In Figure 6 we illustrate several evolutionary tracks for the SMBHs in our sample, since $z = 20$. The simplest scenario assumes that each SMBH grows with a constant L/L_{Edd}, fixed to the observed value. The points where each of the (diagonal solid) lines crosses the y-axis of the *left* panel of Figure 6 may be considered as the implied (seed) BH mass at $z = 20$, under these assumptions. The $z \simeq 2.4$ sources have high-enough accretion rates to account for their observed masses, even if one assumes that they originate from "stellar" BH seeds ($M_{seed} \lesssim 100 M_\odot$) and/or a fractional duty cycle for accretion. Among the $z \simeq 3.3$ sources, however, we see some evidence for either more massive seeds and/or higher accretion rates in yet earlier epochs, as the implied seed masses are typically of order $M_{seed} \sim 10^5 M_\odot$. To illustrate the effect of having higher L/L_{Edd} at earlier epochs, we repeated the calculation of evolutionary tracks, this time assuming that L/L_{Edd} increases with redshift, as suggested by several studies of higher-luminosity AGNs (see Figure 4, and also De Rosa et al. 2014). We assume two very simple evolutionary trends, of the form $L/L_{Edd} \propto (1+z)$ and $L/L_{Edd} \propto (1+z)^2$, both capped at the Eddington limit (i.e., $L/L_{Edd} \leq 1$). The stronger evolutionary trend is consistent with a fit to all the data points in the bottom panel of Figure 4. The results of this latter calculation are illustrated as dashed lines in Figure 6.

[24] These calculations suggest that massive seeds are required to explain *some* $z \simeq 3.3$ sources, even under these favorable conditions. The only scenario in which all the implied seed masses are in the "stellar" regime is indeed the one with the strongest evolution in accretion rates, $L/L_{Edd} \propto (1+z)^2$. We note, however, that all these calculations assume continuous growth, i.e. a duty cycle of 100%. Any other, more realistic choice for the duty cycle, as well as the indirect evidence for somewhat elevated radiative efficiencies for some of the AGNs (Section 3.3), would further challenge the ability of stellar BH seeds to account for the observed BH masses.

Another interesting point that is clearly evident from Figure 6 is that most of the SMBHs studied here *cannot* be considered as the descendants of the known higher-redshift SMBHs. This is due to the simple fact that the observed masses of the $z \simeq 3.3$ SMBHs are lower than, or comparable to, those of the higher-redshift ones. The only exception for this interpretation (except for CID-947) would be a scenario where the lowest-mass SMBHs at $z \simeq 6.2$ would shut off their accretion within a very short timescale, and then be briefly "re-activated" at $z \sim 3.5$. However, given the large difference between the number densities of the population from which our sample is drawn and that of the higher-redshift, higher-luminosity samples shown in Figure 6 (e.g., McGreer et al. 2013), this scenario is unlikely.

The evolutionary tracks we calculate for our $z \simeq 3.3$ sources, combined with the associated number density of their

[24] As for the maximal allowed L/L_{Edd}, we note that few of the $z \simeq 6.2$ and $z \simeq 4.8$ sources have observed accretion rates above the Eddington limit, but those could well be due to the uncertainties related to L/L_{Edd} estimation.

parent population, strongly support the existence of a significant population of relatively low-mass ($M_{\rm BH}\sim10^{6-7}\,M_{\odot}$), active SMBHs at $z\sim5-7$. Moreover, as the right panel of Figure 6 shows, such sources should be observable, as their luminosities are expected to exceed the flux limits of existing deep X-ray surveys, such as the *Chandra COSMOS Legacy* survey itself, or the 4 Ms CDF-S survey (Xue et al. 2011). However, very few such sources are indeed detected. Several surveys of optically selected, unobscured AGNs at $z\sim5-7$ suggest number densities of order $10^{-8}\,{\rm Mpc}^{-3}$ (e.g., McGreer et al. 2013; Kashikawa et al. 2015, and references therein). Even when combining all currently available X-ray surveys, and including *all* sources with redshifts $z\sim5$, the number density of the sources that have comparable luminosities to what we predict here ($\log L_{2-10}\sim43-43.5$) is roughly $\sim5\times10^{-7}\,{\rm Mpc}^{-3}$. In particular, the recent study of Marchesi et al. (2015) identified about 30 X-ray AGNs at $z>4$, based on the same X-ray *Chandra* data used for the selection of the sample studied here. Of these sources, nine are at $z>5$ and only four are at $z\geq6$, with the vast majority of such high-z sources having only photometric redshift estimates. In terms of the typical luminosities of these AGNs, the right panel of Figure 6 clearly shows that the $z\sim5$ X-ray AGNs can indeed be considered as the parent population of our sources. However, the number density of such high-z AGNs is significantly lower than that of our sample. The Marchesi et al. study shows that the cumulative number density of X-ray-selected AGNs drops dramatically with increasing redshift, to reach $\Phi\sim5\times10^{-7}\,{\rm Mpc}^{-3}$ by $z\simeq5$ (split roughly equally between obscured and unobscured AGNs), and to about $10^{-7}\,{\rm Mpc}^{-3}$ by $z\sim6$. This is about an order of magnitude lower than what we consider for the $z\sim6$ progenitors of our sources. This discrepancy is *not* driven by the (X-ray) flux limit of the *Chandra COSMOS Legacy* survey. Indeed, the study of Weigel et al. (2015) did not identify any (X-ray-selected) $z\gtrsim5$ AGNs in the 4 Ms CDF-S data, the deepest available survey (Xue et al. 2011).[25] As illustrated in the right panel of Figure 6, the 4 Ms CDF-S data should have easily detected the progenitors of our sources. We note that the lack of such higher-redshift sources is *not* due to the small size of the CDF-S survey, because it does contain some high-luminosity AGNs at $z\sim5$. In principle, given the general behavior of luminosity functions, the lower-luminosity progenitors of our $z\simeq3.3$ AGNs should have been even more numerous. We conclude that our sample provides compelling evidence for the existence of a significant population ($\Phi\sim10^{-6}\,{\rm Mpc}^{-3}$) of faint $z\sim5-6$ AGNs, powered by SMBHs with $M_{\rm BH}\sim10^{6-7}\,M_{\odot}$ and $L_{\rm bol}\sim(1-3)\times10^{44}\,{\rm erg\,s}^{-1}$, which, however, is not detected (at sufficiently large numbers) in the currently available deep X-rays surveys. We note that while the decline in the number density of AGNs at $z>3$ was well established in several previous studies, including those based on *Chandra* data in COSMOS (Civano et al. 2011, M15), our analysis clearly demonstrates that such "progenitor" AGNs are *expected*, given the masses and accretion rates of the $z\simeq3.3$ AGNs.

There are several possible explanations for this apparent discrepancy between the expected and observed number of $z\gtrsim5$ AGNss:

i. First, the small number of detected "progenitor" systems can be explained by a high fraction of obscured AGNs ($f_{\rm obs}$). If the obscuration of each accreting SMBH evolves with the luminosity of the central source, then we should expect that a certain fraction of the progenitors of our sources would be obscured at earlier epochs. Such a scenario is expected within the framework of "receding torus" models (e.g., Lawrence 1991), where lower luminosities are typically associated with a higher $f_{\rm obs}$. However, several recent studies show that there is little observational evidence in support of such torus models (see, e.g., Oh et al. 2015; Netzer et al. 2016, and Netzer 2015 for a recent review). There is, however, somewhat stronger evidence for an increase in the typical $f_{\rm obs}$ toward high redshifts (e.g., Treister & Urry 2006; Hasinger 2008), perhaps in concert with an increasing frequency of major galaxy mergers (e.g., Treister et al. 2010). A more plausible scenario is therefore that the progenitors of our $z\simeq3.3$ AGNs are embedded in dusty galaxy merger environments with high-column density.

ii. Second, it is possible that, early on, our sources grew with lower radiative efficiencies, which would result in yet-lower luminosities per given (physical) accretion rate. To illustrate the possible effects of lower η on the projected evolutionary tracks of our sources, we repeated the aforementioned evolutionary calculations with $\eta=0.05$ (comparable to the lowest possible value within the standard model of a thin accretion disk). Indeed, at $z\gtrsim5$ the expected luminosities are significantly lower than those projected under the fiducial assumptions. The differences amount to at least an order of magnitude at $z\sim5$, and at least a factor of 30 at $z\sim6$, making most of these projected progenitors undetectable even in the deepest surveys. In this context, we recall that the efficiencies we infer for the sources are actually somewhat *higher* than standard ($\eta\simeq0.15$; Section 3.3). However, lower efficiencies at earlier times may still be expected if one assumes, for example, a relatively prolonged accretion episode that (gradually) "spins up" the SMBHs (e.g., Dotti et al. 2013, and references therein) or supercritical accretion through "slim" accretion disks (e.g., Madau et al. 2014).

iii. Finally, the discrepancy may be explained in terms of the AGN duty cycle, on either long (host-scale fueling) or short (accretion flow variability) timescales. In the present context, this would require that high-redshift, lower-luminosity AGNs would have a lower duty cycle than their (slightly) lower-redshift descendants. We note that such a scenario would actually further complicate the situation, as the growth of the SMBHs would be slower. This, in turn, would mean that our sources should be associated with progenitors of yet higher luminosity at $z\gtrsim5$, which have yet lower number densities.

We conclude that the simplest explanation for the discrepancy between the observed and expected properties of the progenitors of our $z\simeq3.3$ AGNs is probably due to a combination

[25] Another recent study by Giallongo et al. (2015) did claim to identify several $z>4$ sources in the CDF-S field. However, their technique for identifying X-ray sources goes far beyond the standard procedures used in the X-ray luminosity function studies we refer to here, and may introduce false detections.

of an evolution in the radiative efficiencies and/or obscuration fractions, during the growth of individual systems. We stress that such trends are beyond the scope of most "synthesis models," which assume time-invariable accretion rates, radiative efficiencies, and/or obscuration fractions (e.g., Ueda et al. 2014; Georgakakis et al. 2015, and references therein).

4. SUMMARY AND CONCLUSION

We have presented new Keck/MOSFIRE *K*-band spectra for a total of 14 unobscured, $z \sim 2.1-3.7$ AGNs, selected through the extensive *Chandra* X-ray coverage of the COSMOS field. We mainly focus on 10 objects at $z \simeq 3.3$, representing a parent population with a number density of roughly $10^{-6}-10^{-5}\,\mathrm{Mpc}^{-3}$ - a factor of ~ 25 more abundant than previously studied samples of AGNs at these high redshifts. The new data enabled us to measure the black hole masses ($M_{\rm BH}$) and accretion rates (both in terms of $L/L_{\rm Edd}$ and $\dot{M}_{\rm AD}$) for these sources, and to trace their early growth. Our main findings are as follows:

1. The $z \simeq 3.3$ AGNs are powered by SMBHs with typical masses of $M_{\rm BH} \sim 5\times10^8\,M_\odot$ and accretion rates of $L/L_{\rm Edd} \sim 0.1-0.4$. These BH masses are significantly lower than those found for higher-luminosity AGNs at comparable redshifts. Our sample generally lacks AGNs powered by high-mass but slowly accreting SMBHs (i.e., $L/L_{\rm Edd} < 0.1$), although such systems are well within our chosen flux limit. Assuming a standard, thin accretion disk, the data suggest somewhat higher-than-typical radiative efficiencies, of about $\eta \sim 0.15$, in agreement with several recent studies.

2. Assuming continuous growth at the observed accretion rates, most of the $z \simeq 3.3$ SMBHs had to grow from massive BH seeds (i.e., $M_{\rm seed} > 10^4\,M_\odot$). Stellar seeds can only account for the observed masses if $L/L_{\rm Edd}$ was higher at yet earlier epochs. However, invoking any reasonable duty cycle for the accretion, as well as the indirect evidence for somewhat higher-than-standard radiative efficiencies, further complicates the scenario of stellar BH seeds.

3. Our analysis predicts the existence of a large population of $z \sim 6-7$ AGNs, with $\Phi \sim 10^{-5}\,\mathrm{Mpc}^{-3}$, $M_{\rm BH} \sim 10^6\,M_\odot$, and $L_{2-10} \gtrsim 10^{43}\,\mathrm{erg\,s^{-1}}$. Such sources are not detected in sufficiently large numbers in the existing deep X-ray surveys, perhaps because of increased obscuration at high redshift and/or because of lower radiative efficiences in the early stages of black hole growth.

4. Two of the $z \simeq 3.3$ sources, and possibly one additional source ($\sim 17-25\%$) have extremely weak broad Hβ emission components, although their (archival) optical spectra clearly show strong emission from other, high-ionization broad lines (e.g., C IV). The weakness of the broad Hβ lines *cannot* be due to dust obscuration along the line of sight, nor due to the lack of BLR gas. A sudden decrease in AGN (continuum) luminosity is also improbable. Another source shows a peculiarly broad [O III] profile. Repeated optical spectroscopy of these sources may clarify the physical mechanisms that drive the highly unusual broad-line emission.

5. One source in our sample, the broad-absorption-line AGN CID-947, has a significantly higher $M_{\rm BH}$ and lower $L/L_{\rm Edd}$ than the rest of the sample. Our detailed analysis (published separately as Trakhtenbrot et al. 2015) suggests that the SMBH in this system is at the final phase of growth. Compared with the rest of the sample analyzed here, CID-947 appears to be an outlier in the general distributions of $M_{\rm BH}$ and $L/L_{\rm Edd}$. We stress, however, that it is highly unlikely that systems like CID-947 are extremely rare, as we have identified one such object among a sample of ten.

Our sample presents preliminary insights into key properties of *typical* SMBHs at $z \simeq 3.3$. Clearly, a larger sample of faint AGNs is needed in order to establish the black hole mass function and accretion rate function at this early cosmic epoch. We are pursuing these goals by relying on the (relatively) unbiased selection function enabled by deep X-ray surveys, in extragalactic fields where a rich collection of supporting multi-wavelength data are available. A forthcoming publication will explore the host galaxies of the AGNs studied here, and trace the evolution of the well-known SMBH-host scaling relations to $z \sim 3.5$.

We thank the anonymous referee, whose numerous suggestions helped improve the paper. The new MOSFIRE data presented here were obtained at the W. M. Keck Observatory, which is operated as a scientific partnership among the California Institute of Technology, the University of California, and the National Aeronautics and Space Administration. The Observatory was made possible by the generous financial support of the W. M. Keck Foundation. We are grateful for the support from Yale University that allows access to the Keck telescopes. We thank M. Kassis, L. Rizzi, and the rest of the staff at the W. M. Keck observatories at Waimea, HI, for their support during the observing runs. We recognize and acknowledge the very significant cultural role and reverence that the summit of Mauna Kea has always had within the indigenous Hawaiian community. We are most fortunate to have the opportunity to conduct observations from this mountain. Some of the analysis presented here is based on data products from observations made with European Southern Observatory (ESO) Telescopes at the La Silla Paranal Observatory under ESO program ID 179.A-2005 and on data products produced by TERAPIX and the Cambridge Astronomy Survey Unit on behalf of the UltraVISTA consortium. This work made use of the MATLAB package for astronomy and astrophysics (Ofek 2014). We thank A. Weigel and N. Caplar for beneficial discussions. F.C. and C.M.U. gratefully thank Debra Fine for her support of women in science. This work was supported in part by NASA *Chandra* grant numbers GO3-14150C and GO3-14150B (F.C., S.M., H.S., M.E.). K.S. gratefully acknowledges support from Swiss National Science Foundation Grant PP00P2_138979/1. J.M. acknowledges support for his PhD by CONICYT-PCHA/doctorado Nacional para extranjeros, scholarship 2013-63130316. A.F. acknowledges support from the Swiss National Science Foundation.

REFERENCES

Abazajian, K. N., AdelmanMcCarthy, J. K., Agüeros, M. a., et al. 2009, ApJS, 182, 543 [1]

Agarwal, B., Davis, A. J., Khochfar, S., Natarajan, P., & Dunlop, J. S. 2013, MNRAS, 432, 3438 [1]

Aird, J., Coil, A. L., Georgakakis, A., et al. 2015, MNRAS, 451, 1892 [1]
Alexander, D. M., Brandt, W. N., Smail, I., et al. 2008, AJ, 135, 1968 [3.2]
Alexander, T., & Natarajan, P. 2014, Science, 345, 1330 [1]
Baldwin, J. A., Phillips, M. M., & Terlevich, R. 1981, PASP, 93, 5 [3.1]
Banerji, M., Alaghband-Zadeh, S., Hewett, P. C., & McMahon, R. G. 2015, MNRAS, 447, 3368 [2.1, 3.2]
Baskin, A., & Laor, A. 2005, MNRAS, 356, 1029 [1]
Bentz, M. C., Denney, K. D., Grier, C. J., et al. 2013, ApJ, 767, 149 [2.5]
Bongiorno, A., Maiolino, R., Brusa, M., et al. 2014, MNRAS, 443, 17 [3.2]
Bonoli, S., Mayer, L., & Callegari, S. 2014, MNRAS, 437, 1576 [1]
Boroson, T. A., & Green, R. F. 1992, ApJS, 80, 109 [2.4, 3.1]
Brandt, W. N., & Alexander, D. M. 2015, A&ARv, 23, 1 [1]
Brusa, M., Comastri, A., Gilli, R., et al. 2009, ApJ, 693, 8 [1, 2.3]
Brusa, M., Civano, F. M., Comastri, A., et al. 2010, ApJ, 716, 348 [2.1]
Capak, P. L., Aussel, H., Ajiki, M., et al. 2007, ApJS, 172, 99 [1]
Civano, F. M., Brusa, M., Comastri, A., et al. 2011, ApJ, 741, 91 [1, 3.4]
Civano, F. M., Elvis, M., Brusa, M., et al. 2012, ApJS, 201, 30 [2.1]
Civano, F., Marchesi, S., Comastri, A., et al. 2016, ApJ, 819, 62 [1, 2.1, 1]
Collin, S., Boisson, C., Mouchet, M., et al. 2002, A&A, 388, 771 [3.3]
Comerford, J. M., Gerke, B. F., Stern, D., et al. 2012, ApJ, 753, 42 [3.1]
Cushing, M. C., Vacca, W. D., & Rayner, J. T. 2004, PASP, 116, 362 [2.2]
Davis, S. W., & Laor, A. 2011, ApJ, 728, 98 [3.3, 3.3]
De Rosa, G., Decarli, R., Walter, F., et al. 2011, ApJ, 739, 56 [1, 3.2]
De Rosa, G., Venemans, B. P., Decarli, R., et al. 2014, ApJ, 790, 145 [1, 3.2, 3.4]
Denney, K. D., Peterson, B. M., Dietrich, M., Vestergaard, M., & Bentz, M. C. 2009, ApJ, 692, 246 [2.4]
Denney, K. D., De Rosa, G., Croxall, K., et al. 2014, ApJ, 796, 134 [3.1]
Dietrich, M., Mathur, S., Grupe, D., & Komossa, S. 2009, ApJ, 696, 1998 [1, 3.2]
Dijkstra, M., Haiman, Z., Mesinger, A., & Wyithe, J. S. B. 2008, Monthly Notices of the Royal Astronomical Society, 391, 1961 [1]
Dotti, M., Colpi, M., Pallini, S., Perego, A., & Volonteri, M. 2013, ApJ, 762, 68 [2]
Elvis, M., Risaliti, G., & Zamorani, G. 2002, ApJL, 565, L75 [3.3]
Elvis, M., Civano, F. M., Vignali, C., et al. 2009, ApJS, 184, 158 [1, 2.1, 1]
Fevre, O. L., Cassata, P., Cucciati, O., et al. 2013, A&A, 559, A14 [1]
Fine, S., Croom, S. M., Bland-Hawthorn, J., et al. 2010, MNRAS, 409, 591 [1]
Fiore, F., Grazian, A., Santini, P., et al. 2008, ApJ, 672, 94 [2.1]
Gavignaud, I., Wisotzki, L., Bongiorno, A., et al. 2008, A&A, 492, 637 [3.2]
Georgakakis, A., Aird, J., Buchner, J., et al. 2015, MNRAS, 453, 1946 [1, 3.4]
Giallongo, E., Grazian, A., Fiore, F., et al. 2015, A&A, 578, A83 [25]
Gilli, R., Comastri, A., & Hasinger, G. 2007, A&A, 463, 79 [1]
Glikman, E., Bogosavljević, M., Djorgovski, S. G., et al. 2010, ApJ, 710, 1498 [1]
Glikman, E., Simmons, B. D., Mailly, M., et al. 2015, ApJ, 806, 218 [2.1, 3.2]
Greene, J. E., & Ho, L. C. 2005, ApJ, 630, 122 [2.1, 2.5]
Greene, J. E., & Ho, L. C. 2007, ApJ, 667, 131 [2.5]
Grier, C. J., Martini, P., Watson, L. C., et al. 2013, ApJ, 773, 90 [2.5]
Hasinger, G. 2008, A&A, 490, 905 [1]
Hasinger, G., Miyaji, T., & Schmidt, M. 2005, A&A, 441, 417 [1]
Hasinger, G., Cappelluti, N., Brunner, H., et al. 2007, ApJS, 172, 29 [2.1]
Ikeda, H., Nagao, T., Matsuoka, K., et al. 2011, ApJL, 728, L25 [1]
Jiang, L., Fan, X., Hines, D. C., et al. 2006, AJ, 132, 2127 [23]
Kashikawa, N., Ishizaki, Y., Willott, C. J., et al. 2015, ApJ, 798, 28 [3.4]
Kaspi, S., Maoz, D., Netzer, H., et al. 2005, ApJ, 629, 61 [2.5, 2.5]
Kaspi, S., Smith, P. S., Netzer, H., et al. 2000, ApJ, 533, 631 [2.5]
Kellermann, K. I., Sramek, R., Schmidt, M., Shaffer, D. B., & Green, R. F. 1989, AJ, 98, 1195 [2.3]
Kewley, L. J., Groves, B., Kauffmann, G., & Heckman, T. M. 2006, MNRAS, 372, 961 [3.1]
Komossa, S., Xu, D., Zhou, H., Storchi-Bergmann, T., & Binette, L. 2008, ApJ, 680, 926 [3.1]
Kormendy, J., & Ho, L. C. 2013, ARA&A, 51, 511 [1]
Kurk, J. D., Walter, F., Fan, X., et al. 2007, ApJ, 669, 32 [1, 3.2, 4]
LaMassa, S. M., Cales, S., Moran, E. C., et al. 2015, ApJ, 800, 144 [3.1]
Lawrence, A. 1991, MNRAS, 252, 586 [1]
Lilly, S. J., Fevre, O. L., Renzini, A., et al. 2007, ApJS, 172, 70 [2.1, 1]
Lilly, S. J., Le Brun, V., Maier, C., et al. 2009, ApJS, 184, 218 [2.1]
Lusso, E., Comastri, A., Vignali, C., et al. 2010, A&A, 512, A34 [2.5]
Lusso, E., Comastri, A., Vignali, C., et al. 2011, A&A, 534, A110 [2.5]
Madau, P., Haardt, F., & Dotti, M. 2014, ApJL, 784, L38 [1, 2]
Marchesi, S., Civano, F. M., Elvis, M., et al. 2015, ApJ, submitted [1, 2, 3.4]
Marchesi, S., Civano, F., Elvis, M., et al. 2016, ApJ, 817, 34 [2.1, 2.3]
Marconi, A., Risaliti, G., Gilli, R., et al. 2004, MNRAS, 351, 169 [1, 2.5, 2.5, 6]
Marziani, P., Sulentic, J. W., Stirpe, G. M., Zamfir, S., & Calvani, M. 2009, A&A, 495, 83 [1, 2.5, 3.1, 3.2]
Masters, D., Capak, P. L., Salvato, M., et al. 2012, ApJ, 755, 169 [1, 2.1, 1]
McConnell, N. J., Ma, C.-p., Gebhardt, K., et al. 2011, Nature, 480, 215 [1]
McCracken, H. J., Milvang-Jensen, B., Dunlop, J. S., et al. 2012, A&A, 544, A156 [2.1, 1, 23]
McGreer, I. D., Jiang, L., Fan, X., et al. 2013, ApJ, 768, 105 [1, 3.4]
McLean, I. S., Steidel, C. C., Epps, H. W., et al. 2012, Proc. SPIE, 8446, 84460J [2.2]
McLure, R. J., & Dunlop, J. S. 2004, MNRAS, 352, 1390 [3.2]
McLure, R. J., & Jarvis, M. J. 2004, MNRAS, 353, L45 [2.3]
Mejia-Restrepo, J. E., Trakhtenbrot, B., Lira, P., Netzer, H., & Capellupo, D. M. 2016, MNRAS, in press, arXiv:1603.03437 []
Miyaji, T., Hasinger, G., Salvato, M., et al. 2015, ApJ, 804, 104 [1]
Morganson, E., Burgett, W. S., Chambers, K. C., et al. 2014, ApJ, 784, 92 [2.2]
Natarajan, P. 2011, BASI, 39, 145 [1]
Netzer, H. 2015, ARA&A, 53, 365 [1]
Netzer, H., Lani, C., Nordon, R., et al. 2016, ApJ, 819, 123 [1]
Netzer, H., Lira, P., Trakhtenbrot, B., Shemmer, O., & Cury, I. 2007, ApJ, 671, 1256 [1, 2.1, 1, 2.5, 3.1, 3.2, 4, 5]
Netzer, H., & Trakhtenbrot, B. 2014, MNRAS, 438, 672 [3.3, 3.3]
Ofek, E. O. 2014, Astrophysics Source Code Library, ascl: 1407.005 [4]
Oh, K., Yi, S. K., Schawinski, K., et al. 2015, ApJS, 219, 1 [1]
Onken, C. a., Ferrarese, L., Merritt, D., et al. 2004, ApJ, 615, 645 [2.5]
Plotkin, R. M., Shemmer, O., Trakhtenbrot, B., et al. 2015, ApJ, 805, 123 [3.1]
Reynolds, C. S. 2014, SSRv, 183, 277 [3.3]
Reynolds, M. T., Walton, D. J., Miller, J. M., & Reis, R. C. 2014, ApJL, 792, L19 [3.3]
Richards, G. T., Strauss, M. A., Fan, X., et al. 2006, AJ, 131, 2766 [1]
Runnoe, J. C., Cales, S., Ruan, J. J., et al. 2016, MNRAS, 455, 1691 [3.1]
Schawinski, K., Urry, C. M., Treister, E., et al. 2011, ApJL, 743, L37 [1]
Schinnerer, E., Sargent, M. T., Bondi, M., et al. 2010, ApJS, 188, 384 [2.3]
Schulze, A., Bongiorno, A., Gavignaud, I., et al. 2015, MNRAS, 447, 2085 [3.2]
Scoville, N. Z., Aussel, H., Brusa, M., et al. 2007, ApJS, 172, 1 [1]
Shakura, N. I., & Sunyaev, R. A. 1973, A&A, 24, 337 [3.3]
Shang, Z., Wills, B. J., Wills, D., & Brotherton, M. S. 2007, AJ, 134, 294 [2.4]
Shemmer, O., Netzer, H., Maiolino, R., et al. 2004, ApJ, 614, 547 [1, 2.1, 1, 2.5, 3.1, 3.2, 4, 5]
Shemmer, O., Trakhtenbrot, B., Anderson, S. F., et al. 2010, ApJL, 722, L152 [3.1]
Shen, Y. 2013, BASI, 41, 61 [2.1, 2.2, 2.5]
Shen, Y., Greene, J. E., Strauss, M. A., Richards, G. T., & Schneider, D. P. 2008, ApJ, 680, 169 [1]
Shen, Y., & Liu, X. 2012, ApJ, 753, 125 [1]
Shen, Y., Richards, G. T., Strauss, M. a., et al. 2011, ApJS, 194, 45 [2.4, 3.1]
Siana, B., del Carmen Polletta, M., Smith, H. E., et al. 2008, ApJ, 675, 49 [1]
Silverman, J. D., Mainieri, V., Salvato, M., et al. 2010, ApJS, 191, 124 [1]
Suh, H., Hasinger, G., Steinhardt, C. L., Silverman, J. D., & Schramm, M. 2015, ApJ, 815, 129 [3.2]
Szokoly, G. P., Bergeron, J., Hasinger, G., et al. 2004, ApJS, 155, 271 [1]
Tilton, E. M., & Shull, J. M. 2013, ApJ, 774, 29 [1]
Trakhtenbrot, B. 2014, ApJL, 789, L9 [3.3]
Trakhtenbrot, B., & Netzer, H. 2012, MNRAS, 427, 3081 [1, 2.1, 2.4, 2.5, 2.5, 3.1, 3.2]
Trakhtenbrot, B., Netzer, H., Lira, P., & Shemmer, O. 2011, ApJ, 730, 7 [1, 3.2, 4]
Trakhtenbrot, B., Urry, C. M., Civano, F. M., et al. 2015, Science, 349, 168 [1, 4, 5]
Treister, E., Natarajan, P., Sanders, D. B., et al. 2010, Science, 328, 600 [1]
Treister, E., & Urry, C. M. 2006, ApJL, 652, L79 [1]
Treister, E., Urry, C. M., & Virani, S. N. 2009a, ApJ, 696, 110 [1]
Treister, E., Cardamone, C. N., Schawinski, K., et al. 2009b, ApJ, 706, 535 [2.1]
Trump, J. R., Impey, C. D., Kelly, B. C., et al. 2009a, ApJ, 700, 49 [3.2]
Trump, J. R., Impey, C. D., Elvis, M., et al. 2009b, ApJ, 696, 1195 [1, 2.1, 1]
Ueda, Y., Akiyama, M., Hasinger, G., Miyaji, T., & Watson, M. G. 2014, ApJ, 786, 33 [1, 3.4]
Vacca, W. D., Cushing, M. C., & Rayner, J. T. 2003, PASP, 115, 389 [2.2]
Vanden Berk, D. E., Richards, G. T., Bauer, A. E., et al. 2001, AJ, 122, 549 [2.1, 2.5]
Vanden Berk, D. E., Wilhite, B. C., Kron, R. G., et al. 2004, ApJ, 601, 692 [2.2]
Vestergaard, M., & Peterson, B. M. 2006, ApJ, 641, 689 [2.5]
Vito, F., Gilli, R., Vignali, C., et al. 2014, MNRAS, 445, 3557 [1]
Vito, F., Vignali, C., Gilli, R., et al. 2013, MNRAS, 428, 354 [1, 6]
Volonteri, M. 2010, The A&ARv, 18, 279 [1]
Wang, F., Wu, X.-B., Fan, X., et al. 2015, ApJL, 807, L9 [3.2]
Weigel, A. K., Schawinski, K., Treister, E., et al. 2015, MNRAS, 448, 3167 [3.4]
Wilhite, B. C., Brunner, R. J., Grier, C. J., Schneider, D. P., & Vanden Berk, D. E. 2008, MNRAS, 383, 1232 [2.2]
Willott, C. J., Albert, L., Arzoumanian, D., et al. 2010, AJ, 140, 546 [1, 4, 3.2]
Woo, J.-H., Treu, T., Barth, A. J., et al. 2010, ApJ, 716, 269 [2.5]
Wu, X.-B., Wang, F., Fan, X., et al. 2015, Nature, 518, 512 [3.2]
Xue, Y. Q., Luo, B., Brandt, W. N., et al. 2011, ApJS, 195, 10 [1, 3.4]